A comprehensive experimental and numerical analysis of water flow and travel time in a highly heterogeneous vadose zone

Arnaud Isch, Yves Coquet, Bouamama Abbar, Carlos Aldana, Mohamad
Abbas, Ary Bruand, Mohamed Azaroual

▶ **To cite this version:**

HAL Id: insu-03654372
https://insu.hal.science/insu-03654372

Submitted on 28 Apr 2022

Journal Pre-proofs

Arnaud Isch, Yves Coquet, Bouamama Abbar, Carlos Aldana, Mohamad Abbas, Ary Bruand, Mohamed Azaroual

Please cite this article as: Isch, A., Coquet, Y., Abbar, B., Aldana, C., Abbas, M., Bruand, A., Azaroual, M., A comprehensive experimental and numerical analysis of water flow and travel time in a highly heterogeneous vadose zone, *Journal of Hydrology* (2022), doi: https://doi.org/10.1016/j.jhydrol.2022.127875
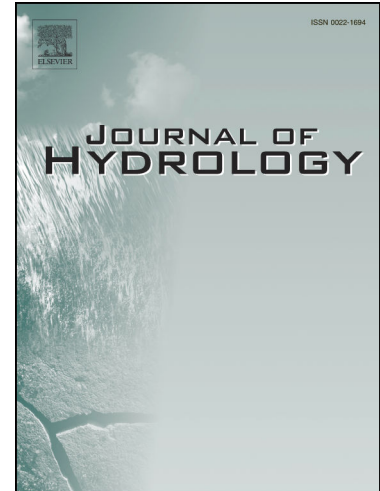
A comprehensive experimental and numerical analysis of water flow and travel time in a

highly heterogeneous vadose zone

Arnaud Isch[1]*, Yves Coquet[2], Bouamama Abbar[1], Carlos Aldana[1], Mohamad Abbas[1], Ary Bruand[1], Mohamed Azaroual[1,3]

[1] Université d'Orléans, BRGM, ISTO UMR 7327, 1A rue de la Ferollerie, 45071 Orléans, France

[2] ECOSYS UMR 1402, AgroParisTech, INRAE, Université Paris Saclay, 78850 Thiverval-Grignon, France

[3] BRGM, 3 avenue Claude-Guillemin, BP 6009, 45060 Orléans, France.

* Corresponding author (arnaud.isch@gmail.com)

Abbreviations: BBC, Burdine-Brooks & Corey; CZ, critical zone; DBM, Durner bimodal model; ETP, reference Penman-Monteith potential evapotranspiration; MVG, Mualem-van Genuchten; R, rainfall; TT, water travel time; WTL, water table level; VZ, vadose zone.

Highlights:

- ✓ Simulation of water flow and TT in the VZ using unimodal and bimodal approaches

- ✓ Parameterization of HYDRUS-1D using hydraulic properties laboratory measurements

- ✓ Experimental hydraulic properties were more accurately described with the DBM model

- ✓ Results obtained with unimodal and bimodal models presented strong differences

- ✓ Large influence of VZ vertical heterogeneity and meteorological conditions

Abstract

The assessment of water travel time through the vadose zone is known to be critical for a proper estimation of the hydrologic response time of water bodies to changes in land use management and global changes. In this study, the hydraulic properties of fifteen samples displaying contrasted lithologies (soil, powdery limestone, calcareous sand, limestone rock) and extracted from three cored boreholes drilled throughout the vadose zone of a vulnerable limestone aquifer were first determined in the laboratory. Three 23 m-deep vadose zone profiles were then reconstituted with the HYDRUS-1D software for the numerical simulation of water flow and the estimation of the water travel time using unimodal and bimodal approaches. The measured hydraulic properties, meteorological and water table level data were used as input for a virtual bromide tracing experiment undertaken over a period of 55 years (1966-2020). The results showed that the experimental hydraulic properties of the samples were more accurately described with a dual porosity approach, since the latter allowed a precise representation of the bimodal characteristic of most of the samples. The water flow and travel time simulated using unimodal or bimodal models for describing the vadose zone hydraulic properties were largely different. The impact of the vadose zone lateral heterogeneities on the simulated water flow and the estimated travel time was relatively limited compared to the influence of the vadose zone vertical heterogeneities and meteorological conditions. The mean travel time of the first concentration, peak concentration and last concentration of bromide simulated with the bimodal model at the maximum water table level of the aquifer was 13.8, 20.9 and 31.5 years, respectively. Increase in travel time was clearly identified since the late 1970s, and could be a consequence of global warming. These results also pointed out the need for conducting extensive studies at larger scales to take into account possible fast transfers of water that might occur through open fractures and karst networks.

Keywords:

1. **Introduction**

An increasing number of Earth's Critical Zone (CZ) networks and observatories have emerged in recent years (Gaillardet et al., 2018; Guo and Lin, 2016; Zacharias et al., 2011), stimulated by societal challenges like the prediction of natural hazards, carbon storage or water resources management. These observatories are dedicated to deciphering the complex hydrological and biogeochemical processes which occur at various temporal and spatial scales in the CZ (Bogena et al., 2018; Brantley et al., 2018; Galle et al., 2018; Jensen and Refsgaard, 2018; Li et al., 2018; Molénat et al., 2018; O'Geen et al., 2018; Pisinaras et al., 2018; Seyfried et al., 2018). The Vadose Zone (VZ), which extends from the soil surface down to the aquifer, is considered as a key component of the CZ and is of major importance in the hydrological and biogeochemical cycles. Consequently, an increasing body of work aims at improving the knowledge of the VZ functioning, which includes numerous complex and coupled physical, geochemical, and microbial processes (Aldana et al., 2021; Arora et al., 2019; Vereecken et al., 2016). This constitutes a fundamental milestone for a proper assessment of groundwater recharge and in managing contamination issues for the preservation of aquifers. This is especially true since the increasing use of groundwater resources worldwide and the degradation of the quality of the water resources caused by intensive agriculture have led to the enforcement of several stringent regulatory measures in several countries geared towards achieving a good chemical status for all water bodies in years ahead (Vero et al., 2017).

In this context, the estimation of the water travel time through the VZ is crucial as it constitutes an important component of the total time lag defining the inherent hydrologic response delay

of water bodies to a change in land management practices. This response time is often conceptualized as consisting in both a vertical (within the VZ) and a lateral (within the saturated zone) component (Sousa et al., 2013). The knowledge of the water travel time through the VZ is considered as a prerequisite for quantifying the recharge rate and the time of migration of contaminants from the soil surface down to the aquifer (Mattern and Vanclooster, 2010). However, the water travel time in the VZ is known to be highly variable in space and time. Its quantification is recognized as highly complex and influenced by several factors including the size and geometry of the VZ, the properties of the VZ materials, the physical, chemical and biological processes governing water flow and solute transport within the VZ and the pattern of the meteorological inputs (Jeong et al., 2017; Leij and van Genuchten, 2002; Sousa et al., 2013; Sprenger et al., 2016; Vero et al., 2014). Numerous experimental methods are currently used to estimate the water travel time through the VZ, such as lysimeters (mainly focused on the soil) or field experiments using radioactive or stable isotopes, chloride, nitrate, bromide or fluorobenzoate as tracers (Asadollahi et al., 2020; Chen et al., 2019; Ju et al., 2020; Sprenger et al., 2016; Turkeltaub et al., 2018). However, these experimental approaches are known to be fairly expensive, labor intensive, time consuming and may also have limited predictive capacity. As a consequence, numerical models are being increasingly used for the study of water flow, solute transport and travel time assessments within the VZ (Bouraoui and Grizzetti, 2014; Konikow, 2011; Schoups et al., 2008; Szymkiewicz et al., 2019; Vero et al., 2014). These models need an estimation of the VZ hydrodynamic parameters and may partly rely on pedotransfer functions (Patil and Singh, 2016; Schaap et al., 2001; Szymkiewicz et al., 2018; Vereecken et al., 2010; Vero et al., 2017; Zhang and Schaap, 2019). Some authors used inverse modeling approaches based on transient measurements of water content, matric head and tracer content in the VZ (Haws et al., 2005; Jacques et al., 2002; Sprenger et al., 2016, 2015; Varvaris et al., 2021a, 2021b). However, hydraulic data acquisition is mostly focused on the soil

compartment and the numerical simulations run for the estimation of the travel time are often limited to the use of a unimodal approach, relying notably on the Mualem-van Genuchten model to describe the VZ hydraulic properties (van Genuchten, 1980).

The main objective of this work was to provide a new methodological approach for the study of the water flow and the estimation of the water travel time at the scale of a highly heterogeneous VZ. To this end, the hydraulic properties (water retention and hydraulic conductivity curves) of fifteen samples taken from three cored boreholes and representative of the lithologies (soil, powdery limestone, calcareous sand, limestone rock) encountered within the VZ of a vulnerable limestone aquifer (Beauce, France) were first determined in the laboratory. These experimental data were then used for the parameterization of analytical models describing the measured hydraulic properties using single (unimodal) and dual porosity (bimodal) approaches. The travel time within the VZ has been estimated by means of a virtual bromide tracing experiment performed over a period of 55 years using the HYDRUS-1D software (Šimůnek et al., 2016). The appearance of the initial breakthrough, the peak concentration and the total exit of the tracer at the maximum water table level of the aquifer were considered as indicators of the water travel time. The impact of the choice of the analytical model used to describe the experimental hydraulic properties, the vertical and lateral heterogeneity of the VZ and the meteorological conditions on the simulation of the water flow and travel time through the VZ has been explored.

2. Materials & Methods

2.1. The Beauce limestone aquifer

The multi-layered Beauce limestone aquifer is located in the center of France and extends over 9700 km^2 (de Frutos Cachorro et al., 2017). It is mainly composed of limestones from upper Oligocene to lower Miocene but also consists in clay, marl, powdery limestone, calcareous sand or chalk facies depending on the location. This mostly unconfined aquifer is spread between

the Seine (northeast) and the Loire (southwest) rivers and constitutes one of the largest groundwater reservoirs in France with an average water stock of 20 billion m^3 and high inter-annual variations (Le Coz, 2000). The Beauce represents the main cereal-producing region in Europe (Graveline, 2020). Its land use consists essentially in agriculture (74%), 50% of which is irrigated. Indeed, the region is one of the driest in France with an annual average precipitation of 600 mm (Lejars et al., 2012). This results in an intense irrigated farming of between 120 000 and 240 000 ha that withdraws from the groundwater resource between 150 and 450 million m^3 of water per year (Graveline, 2020). The sensitivity of the water resource to natural recharge and the observation of an overall lowering of the water table level since the early 1990s have led to the implementation of several local water policy measures to control water withdrawals in connection with the French Water Law (Légifrance, 1992), which is now the translation of the European Water Framework Directive (European Commission, 2000). Over the past decades, the Beauce intensive agriculture has also impacted the groundwater quality with nitrates and pesticides (notably atrazine and bentazon) whose concentrations still exceed regulatory limits (DDT, 2016) despite government policies and regulatory measures that have been put into effect since the early 1990s (European Commission, 2009, 1991).

2.2. Location, sampling and description of the VZ materials

The experimental site is located at Villamblain, 30 km northwest of Orléans (France) (DMS coordinates: X = 48°1'5.131"; Y=1°34'55.333"). Three cored boreholes (B1, B2 and B3) separated by a maximum distance of 10.8 m from each other (**Figure 1**) have been drilled in March 2017 from 0 to 20 m deep. The soil formation (0.0-1.5 m deep) was drilled by hydraulic percussion while the other VZ materials (1.5-20.0 m deep) were taken by rotary drilling with a three-annular compartments corer to avoid sample contamination by the drilling fluid (water). As stated by Aldana et al. (2021), compaction caused by hydraulic percussion led to unreliable hydraulic properties data for the soil samples. Consequently, additional soil samples were

collected manually from the ground surface after digging a pit at a few meters from the three boreholes (**Figure 1**) and down to a depth of 1 m.

The VZ lithologies were described based on visual examination of the undisturbed core samples. It revealed a high vertical (within a single borehole) and lateral (between the three boreholes) lithological heterogeneity (Aldana et al., 2021; Isch et al., 2020). A soil with a thickness between 0.9 and 1.8 m was observed at the top of the VZ. This soil is typical of the Beauce region and is referred to as a loamy clay Calcisol (Duval and Isambert, 1992; Michot et al., 2003) according to the French soil reference system (Baize and Girard, 2009), or a Hypereutric Cambisol with a silt loam texture according to the World Reference Base for Soils (IUSS Working Group WRB, 2015). Three main soil layers were observed during the visual description of the core samples and the soil pit (0.0-0.3 m; 0.3-0.6 m; > 0.6 m) (Aldana et al., 2021; Isch et al., 2020). The thickness of the soil layers was in good agreement with that described in other studies carried out near the experimental site (Michot et al., 2003; Ould Mohamed et al., 1997). The soil is developed on a highly heterogeneous Miocene lacustrine fragmented powdery limestone facies (referred to as "powdery limestone" in this work) that has been cryoturbated in its upper part during the Quaternary (Michot et al., 2003; Ould Mohamed and Bruand, 1994) and which also contains calcareous sand interbeds (Aldana et al., 2021). The thickness of this layer is from 5.2 to 6.8 m. Finally, the last main stratigraphic facies is a 12.2 to 13.4 m thick massive, fractured or weathered hard rock (Pithiviers limestone) (Aldana et al., 2021; Schnebelen et al., 1999).
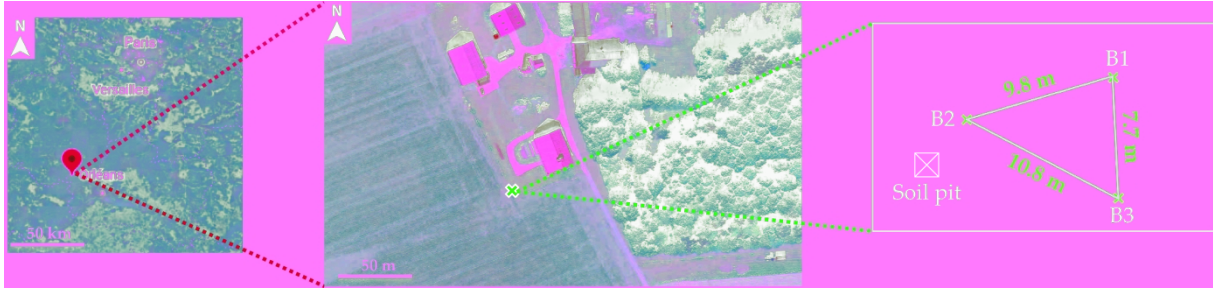
Figure 1: Localization of the experimental site, distance between the three cored boreholes (B1, B2 and B3) and position of the soil pit.

2.3. Climate and water table level data

Meteorological data were collected from the Bricy weather station located about 20 km east of the study site. From 1966 to 2020, the mean annual rainfall (R) and reference Penman-Monteith potential evapotranspiration (ETP) (Monteith, 1965) were of 639.6 mm (± 113.7 mm) and 813.7 mm (± 83.7 mm), respectively. Maximum annual rainfall of 929.8 mm and ETP of 1044.1 mm were observed in 2001 and 2020, respectively (**Figure 2**). Minimum annual rainfall of 413.3 mm and ETP of 658.2 mm were observed in 1990 and 1981, respectively. The climate of the study site is continental-temperate with an mean annual temperature of 11.1°C (± 0.7°C) observed between 1966 and 2020 (minimum of 9.7°C in 1980 and maximum of 12.8°C in 2020). The water table level (WTL) data were collected daily at Poiseaux from a monitoring piezometer situated about 4 km south of the study site. The groundwater recharge displayed an annual dynamics overlaid by multiannual trends (**Figure 2**). From 1966 to 2020, the mean WTL was -18.40 m. The rise of WTL observed from 1999 to the 15/05/2001, which led to a WTL_{MAX} of -14.60 m at that date, was linked to high annual R and R-ETP balance (close to or above 0 mm) over the period. The same trend was observed during other periods corresponding to a rising WTL (1977-1984 and 2012-2014). The lowering of the WTL observed from 1989 to the 19/08/1992, which led to a WTL_{MIN} of -22.21 m at that date, was linked to low annual R and R-ETP balance (below -300 mm) over the period. The same trend was observed during other periods corresponding to a lowering WTL (1970-1974, 2003-2011 and 2017-2020).
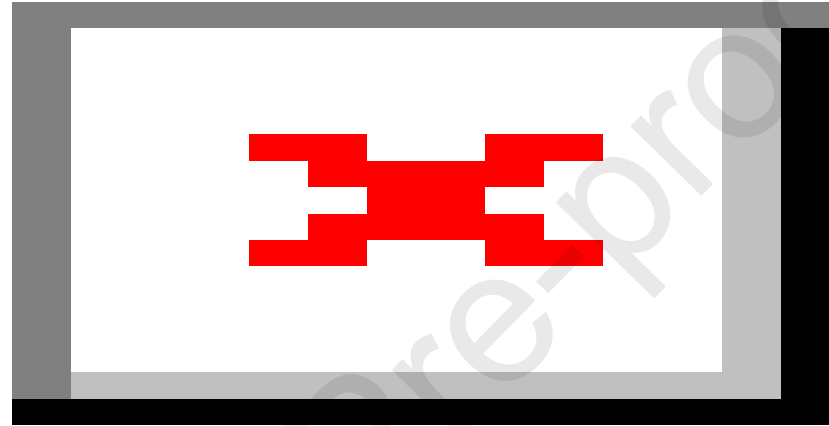
Figure 2: Annual mean temperature, rainfall and ETP, and daily water table level observed from 1966 to 2020.

2.4. Measurements of the hydraulic properties of the vadose zone samples

Following the drilling phase, twelve undisturbed samples representative of the VZ materials were selected from the three cored boreholes, based on the observations made during the lithological description. Three types of lithology were sampled throughout the VZ profile (1-20 m deep) including soft sediments with four powdery limestone samples (P_A, P_B, P_C and P_D) and two calcareous sand samples (I_A and I_B), and hard materials with six limestone rock samples (R_A, R_B, R_C, R_D, R_E and R_F). Additionally, three undisturbed soil samples (S_A, S_B and S_C) were collected from a soil pit. Their hydraulic properties were determined according to the same procedure as for the other VZ samples.

The undisturbed samples were re-cored in the laboratory for adaptation to the experimental device, except sample I_B (calcareous sand deposit) which was repacked to the observed field bulk density. The unsaturated hydraulic properties of the samples, i.e., the water retention curve $\theta(h)$ and the hydraulic conductivity curve $K(h)$, were measured within the pF (log $|h|$, h in cm) value range 0.5-3.0 by means of a triaxial system used by applying the multistep outflow method (Aldana et al., 2021). Calculation of the hydraulic conductivity (K) from outflow data was based on the method given by Gardner (1956) assuming that the matric head in the samples varies linearly with depth. The measurement of the water retention curve was extended to the pF range 4.0-6.0 using the WP4C Dewpoint Potentiometer (METER Group®). A comprehensive description of the measurement system, experimental protocol and calculation methods can be found in Aldana et al. (2021).

The experimental water retention and hydraulic conductivity data were then fitted to the $\theta(h)$ and $K(h)$ curves with three analytical models using the RETC software (van Genuchten et al., 1991). The fitting procedure is described in § 2.5.4.

2.5. Simulation of water flow and solute transport in the vadose zone

2.5.1. Theoretical background and general assumptions

The simulation of water flow and solute transport in the VZ was made using the HYDRUS-1D software (Šimůnek et al., 2016). The one-dimensional vertical water flow in the VZ was described by the Richards equation (Richards, 1931) (1):

$$\frac{\partial \theta}{\partial t} = \frac{\partial}{\partial z}\left[K\left(\frac{\partial h}{\partial z} + 1\right)\right] - S \tag{1}$$

with θ the volumetric water content (cm^3/cm^3), t the time (d), z the coordinate along the vertical axis pointing positively upwards (cm), h the matric head (cm), K the hydraulic conductivity (cm/d) and S a sink term (d^{-1}) which accounts for root water uptake.

We used three analytical models for the description of the hydraulic properties, i.e., the water retention characteristic $\theta(h)$ and the hydraulic conductivity characteristic $K(h)$, of the VZ samples.

The first one is the Mualem-van Genuchten (MVG) model which uses the van Genuchten's expression (van Genuchten, 1980) to describe the water retention curve (2) and the statistical pore connection model established by Mualem (1976) to predict the hydraulic conductivity from the water retention curve (3):

$$\theta(h) = \begin{cases} \theta_r + \dfrac{\theta_s - \theta_r}{\left[1 + |\alpha h|^n\right]^m} & h < 0 \\ \theta_s & h \geq 0 \end{cases} \tag{2}$$

$$\text{with} \qquad m = 1 - \frac{1}{n} \qquad n > 1$$

with θ_r et θ_s respectively the residual and saturated volumetric water content (cm^3/cm^3), α an empirical parameter related to the matric head at the inflection point of the retention curve (cm^{-1}) and n a pore size distribution parameter (-) which determines the slope of the curve at the inflection point.

$$K(h) = K_s S_e^l \left[1 - (1 - S_e^{\frac{1}{m}})^m \right]^2$$

(3)

$$\text{with} \qquad S_e = \frac{\theta - \theta_r}{\theta_s - \theta_r}$$

with K_s the saturated hydraulic conductivity (cm/d), S_e the effective saturation (-) and l a pore

connectivity parameter (-). The latter was fixed at the value of 0.5 (Mualem, 1976).

The second model (BBC) used to describe the hydraulic properties implements the equations

of Brooks and Corey (1966, 1964) to describe the water retention curve (4) and the pore-size

distribution model of Burdine (1953) to predict the hydraulic conductivity (5):

$$S_e = \left\{ \begin{array}{ll} |\alpha h|^{-n} & h < -1/\alpha \\ 1 & h \geq -1/\alpha \end{array} \right.$$

(4)

$$K(h) = K_s S_e^{\frac{2}{n} + l + 2}$$

(5)

The third model is the Durner bimodal expression (DBM) (Durner, 1994) which extends the

unimodal MVG model by considering the porous medium composed of two overlapping

regions and fitting the bimodal behavior of the hydraulic properties by a MVG-type function

for each of the two regions (Köhne et al., 2002; Dimitrov et al., 2014) (6) (7):

$$S_e = w_1 \left[1 + (\alpha_1 h)^{n_1} \right]^{-m_1} + w_2 \left[1 + (\alpha_2 h)^{n_2} \right]^{-m_2}$$

(6)

$$K(S_e) = \frac{(w_1 S_{e_1} + w_2 S_{e_2})^l \left(w_1 \alpha_1 \left[1 - \left(1 - S_{e1}^{l/m_1} \right)^{m_1} \right] + w_2 \alpha_2 \left[1 - \left(1 - S_{e2}^{l/m_2} \right)^{m_2} \right] \right)^2}{(w_1 \alpha_1 + w_2 \alpha_2)^2}$$

(7)

with w_i the weighing factors of the two regions (bimodal pore system) which display separate

hydraulic functions and empirical parameters α_i, n_i, m_i and l (subscript $i=1$ and $i=2$).

The root water uptake model was that of Feddes et al. (1978) with no solute uptake. HYDRUS-

1D implements the same linear interpolation scheme for the water stress response function as

the one used in the SWATRE code (Wesseling and Brandyk, 1985). The water stress response function parameters of grass were used (Taylor and Ashcroft, 1972; Wesseling et al., 1991). The root depth of grass was fixed to 30 cm (Schenk and Jackson, 2002).

The one-dimensional vertical solute transport in the VZ was described by the convection-dispersion equation (CDE) (8):

$$\frac{\partial(\theta C)}{\partial t} = \frac{\partial}{\partial z}\left(\theta D \frac{\partial C}{\partial z}\right) - \frac{\partial(qC)}{\partial z} \tag{8}$$

with C, the solute concentration in liquid phase (g/cm^3), q, the water flux density (cm/d) and D, the hydrodynamic dispersion coefficient (cm²/d) given by Bear (1972) (9):

$$D = \lambda V + \frac{D_0 \tau}{\theta} \tag{9}$$

with λ, the material dispersivity (cm), V, the average water velocity in the pores of the material (cm/d), D_0, the solute molecular diffusion coefficient in pure water (1.584 cm²/d for bromide (Lide, 2004)) and τ, the tortuosity factor in liquid phase (-) given by Millington and Quirk (1961).

2.5.2. Representation of the vadose zone profiles

The VZ profiles were reconstituted in HYDRUS-1D for each of the three boreholes (B1, B2 and B3, **Figure 1**). The lithological heterogeneities along each VZ profile were reproduced based on the visual descriptions of the undisturbed cored samples (Aldana et al., 2021). A 23 m deep profile composed of fourteen (B1) and fifteen (B2 and B3) different materials was created for each borehole (**Table 1**). Each material corresponds to a sample whose hydraulic properties have been determined in the laboratory. The last material (R$_F$) has been extended from the maximum drilling depth (20 m) to the maximum profile depth (23 m) in order to allow the WTL to move below 20 m deep.

The three VZ profiles were vertically discretized using (i) a 1-cm mesh size, from 0 to 1 m deep and from 10 to 0 cm above and from 0 to 10 cm below the limit between two successive materials; (ii) a 2-cm mesh size, from 50 to 10 cm above and from 10 to 50 cm below the limit between two successive materials; (iii) a 5-cm mesh size everywhere else. Ten observations nodes were implemented in the B2 profile. Each observation node was placed at the bottom of a given material and was associated with a specific color (**Table 1**). For the comparisons made between the three boreholes, ten observations nodes were implemented within the three VZ profiles with a specific color assigned to a given borehole (**Table 1**).

2.5.3. Initial and boundary conditions

As the water table level at the time of the start of the simulation was -19.57 m, the initial matric head profile was defined with h_i = -100 cm for -18.57 < z < 0.00 m and h_i varying linearly from -100 to +343 cm from z = -18.57 to z = -23.00 m. At the soil surface, a water flux was imposed as upper boundary condition using daily ETP and rainfall data (atmospheric boundary condition with surface layer (2 cm)). The daily variations of the water table level were used as lower boundary condition (variable pressure head).

For the solute transport modelling, a time-dependent concentration of bromide was applied at the soil surface boundary. More details about the concentration of the bromide in the incoming water are given in § 2.5.5. A Cauchy type condition was imposed at the soil surface with dispersive flux considered negligible and a Neumann type condition was imposed at the lower limit of the VZ profile.

Table 1: Representation of the VZ profile for each borehole (B1, B2 and B3): material number, sample identifier, depth interval and depth of the observation nodes.

	B1				B2					B3		
Material	Sample	Interval [m]	Obs. Node B1-B2-B3 [m]	Material	Sample	Interval [m]	Obs. Node B2 [m]	Obs. Node B1-B2-B3 [m]	Material	Sample	Interval [m]	Obs. Node B1-B2-B3 [m]
1	S_A	0.00-0.30	**0.3**	1	S_A	0.00-0.30	/	**0.3**	1	S_A	0.00-0.30	**0.3**
2	S_B	0.31-0.60	**0.6**	2	S_B	0.31-0.60	/	**0.6**	2	S_B	0.31-0.60	**0.6**
3	S_C	0.61-1.00	**0.9**	3	S_C	0.61-0.90	**0.9**	**0.9**	3	S_C	0.61-1.80	**0.9; 1.2**
4	P_A	1.01-1.40	**1.2**	4	P_A	0.91-1.30	**1.3**	**1.2**	4	P_A	1.81-2.00	/
5	P_B	1.41-3.20	**2.5**	5	P_B	1.31-3.50	**3.5**	**2.5; 3.3**	5	P_B	2.01-2.70	**2.5**
6	P_C	3.21-5.30	**3.3**	6	I_A	3.51-4.10	**4.1**	/	6	P_C	2.71-3.50	**3.3**
7	R_A	5.31-5.60	/	7	P_C	4.11-4.60	/	/	7	R_A	3.51-3.80	/
8	I_B	5.61-6.10	**6.0**	8	I_B	4.61-4.90	/	/	8	I_A	3.81-4.20	/
9	P_D	6.11-7.80	/	9	R_A	4.91-5.20	/	/	9	I_B	4.21-5.00	/
10	R_B	7.81-8.50	**8.0**	8	I_B	5.21-5.50	**5.5**	/	10	P_D	5.01-7.00	**6.0**
11	R_D	8.51-11.00	**10.0.**	10	P_D	5.51-6.60	**6.6**	**6.0**	11	R_B	7.01-8.50	**8.0**
12	R_C	11.01-11.20	/	11	R_B	6.61-9.00	**9.0**	**8.0**	12	R_D	8.51-11.30	**10.0**
11	R_D	11.21-14.00	/	12	R_D	9.01-11.20	**11.2**	**10.0**	13	R_C	11.31-11.50	/
13	R_E	14.01-17.40	**14.6**	13	R_C	11.21-11.40	**11.4**	/	12	R_D	11.51-13.70	/
14	R_F	17.41-23.00	/	12	R_D	11.41-14.00	/	/	14	R_E	13.71-17.00	**14.6**
				14	R_E	14.01-16.00	**14.6**	**14.6**	15	R_F	17.01-23.00	/
				15	R_F	16.01-23.00	/	/				

For the study made on the B2 profile, ten observations nodes were implemented and each of them was placed at the bottom of a given material and associated with a specific color. For the comparisons made between the three boreholes (B1, B2 and B3), ten observations nodes were implemented within the three VZ profiles with a specific color assigned to a given borehole.

2.5.4. Description of the fitting procedure

The RETC software (van Genuchten et al., 1991) was used to fit the $\theta(h)$ and $K(h)$ curves (Eq. 2 to 7) to the measured water retention and hydraulic conductivity data. For the three boreholes, the hydrodynamic parameters for the three analytical models (MVG, BBC and DBM) were obtained according to the following steps.

For the soil samples (S_A, S_B and S_C), initial values of parameters θ_r, θ_s, α, n and K_s were taken from Ould Mohamed et al. (1997). Experimental K_s values have already been obtained in the laboratory (constant-head method) by Ould Mohamed et al. (1997) for soil samples taken between a few tens and hundreds of meters from our experimental site. Since the authors have shown little spatial variability in the hydraulic properties of soils taken within the same pedological layer, the values of K_s of the soil samples S_A, S_B and S_C were fixed to the experimental values given by Ould Mohamed et al. (1997) for three of their soil samples taken within the same layers and at the same depths. For the powdery limestone (P_A, P_B, P_C and P_D) and the calcareous sand samples (I_A and I_B), initial values of parameters θ_r, θ_s, α, n and K_s were obtained by using the Rosetta software (Schaap et al., 2001) based on the particle size distribution and bulk density measured for each sample (Aldana et al., 2021). For the limestone rock samples (R_A, R_B, R_C, R_D, R_E and R_F), initial values of θ_r, α, n were obtained using the results of a study performed near the study site (Amraoui et al., 2017). Initial values of θ_s were obtained from experimental data and initial values of K_s were obtained from the first experimental values of the $K(h)$ curves. Concerning the DBM model, the initial values of parameters α_1, n_1 and α_2, n_2 were chosen according to the shape of the experimental water retention curve measured for each sample. These sets of initial values were then used as input to the RETC software and all the parameters were fitted (except l which was fixed at 0.5). As recommended by Sisson and Genuchten (1991) and Yates et al. (1992), the relative weights of

hydraulic conductivity data against retention data ranged between 0.1 to 1.0. As also recommended by Isch et al. (2019), when a correlation higher than 90% was noted between two fitted parameters, the value of one of them was set to that obtained during the first fitting round and a second round was implemented.

The quality of the RETC fitting procedure was evaluated for each sample by the calculation of the coefficient of determination (R^2) and the Akaike's Information Criterion (AICc) according to Eq. (10) (D'Emilio et al., 2018). When the number of experimental observations are small (for $n/K < 40$), the computation of the AICc is more appropriate than the standard AIC, given the increased relative penalty for small data sets and models with a high number of fitted parameters (Laio et al., 2009; Pham, 2019). It is worth noting that the lowest value of AICc indicates the best fitting efficiency.

$$AICc = n \times \ln\left(\frac{RSS}{n}\right) + 2K + \frac{2K\,(K+1)}{n-K-1} \tag{10}$$

with n, the number of experimental observations (-), K, the number of fitted parameters (-) and RSS, the weighted residual sum of square (-).

The dispersivity (λ) values of the soil and powdery limestone samples were obtained from elution experiments conducted on undisturbed columns by Viel (2016). The dispersivity value of the calcareous sand samples was fixed to the mean of the values reported by Vanderborght and Vereecken (2007) for this type of texture. The dispersivity value of the limestone rock samples was taken from Kurotori et al. (2019).

The values obtained for all the parameters were then used to simulate water flow and bromide transport with HYDRUS-1D from 01/01/1966 to 31/12/2020 (55 years).

2.5.5. Procedure implemented for the estimation of the water travel time within the vadose zone

The water travel time (TT) through the VZ was estimated by a virtual tracing experiment, using bromide as an inert and conservative tracer (Isch et al., 2019) in HYDRUS-1D simulations. The bromide input concentration applied at the soil surface (9.7 g/L) was fixed in accordance with the maximum annual limit of nitrogen from livestock manure that can be applied per hectare in Nitrate Vulnerable Zones in the Centre-Val de Loire region (170 kg N/ha) and calculated following (11):

$$C_{0(Br)} = C_{0(N)} \times \frac{MW_{(Br)}}{MW_{(N)}} \tag{11}$$

with $C_{0(Br)}$, the bromide concentration in liquid phase (g/cm^3), $C_{0(N)}$, the nitrogen concentration in liquid phase (0.0017 g/cm^3), $MW_{(Br)}$, the molecular weight of bromide (79.904 g/mol) and $MW_{(N)}$, the molecular weight of nitrogen (14.0067 g/mol).

As recommended by Szymkiewicz et al. (2019), the solute transport simulation started with a "warm-up" period (of 2 years in our case) during which no solute was added to the soil. A single input of bromide was then applied on the 01/01/1968 with the solute concentration added in rainfall water (with R = 10 mm and ETP = 0 mm on the day of input). With the aim of studying TT variability according to the year of bromide input, simulations were repeated with a single input applied on the first day of each year (e.g., 01/01/1969, 01/01/1970, etc.).

As already recommended by some authors (Fenton et al., 2015, 2011; Szymkiewicz et al., 2019; Vero et al., 2017, 2014; Wang et al., 2012), the water travel time within the VZ was estimated using three indicators including (i) the arrival time of a bromide concentration of 1 mg/L at the WTL$_{MAX}$ (TT$_I$), which was viewed as the initial solute breakthrough (which approximately represents 1% of the bromide peak concentration and 0.01% of the bromide input concentration applied at the soil surface) and consequently reflects initial effects of regulation measures; (ii) the arrival time of bromide peak concentration at the WTL$_{MAX}$ (TT$_P$) (which approximately represents 1% of the input bromide concentration applied at the soil surface), which indicates

the temporal trend of the arrival of the maximum concentration of a conservative solute down to the aquifer; (iii) the time after which a bromide concentration of 1 mg/L is no longer observed at WTL_{MAX} (TT_E), as it represents the maximum residence time of the tracer (total exit) within the VZ and consequently the full effects of regulation measures.

3. Results & Discussion

3.1. Hydraulic properties and hydrodynamic parameters of the VZ samples

3.1.1. Experimental hydraulic properties

The hydraulic properties of a majority of the samples concerned by this work have already been discussed in Aldana et al. (2021). However, considering that the results obtained for all the samples have been further investigated and given that six new samples (S_A, S_B, S_C, P_A, R_C and R_D) have been considered in this work, their experimental hydraulic properties are briefly discussed below.

The experimental hydraulic properties (water retention and hydraulic conductivity) of the S_A and S_B soil samples were relatively similar (**Figure 3a**). The S_C sample displayed lower θ_s and K values between pF 0.0 and 2.0 and a higher water retention between pF 1.5 and 3.0, probably due to the slight increase in clay content observed with depth (Aldana et al., 2021; Ould Mohamed et al., 1997). The shapes of the water retention and hydraulic conductivity curves of the three fragmented powdery limestone samples (P_B, P_C and P_D) were close despite a $\Delta\theta$ observed from pF 0.0 to 3.0 for sample P_C (**Figure 3b**). The cryoturbated unit (P_A), which was described by Ould Mohamed and Bruand (1994), displayed higher K for pF < 1.5 and lower K between pF 2.0 and 3.0 than the three other powdery limestone samples (**Figure 3b**). Its θ values were also in good agreement with those reported by Michot et al. (2003) over the range of pF 1.0-4.2. Water retention of calcareous sand interbeds (I_A and I_B samples) was the lowest among the soft VZ materials for pF > 1.0 (except I_A vs P_C) (**Figure 3c**). I_B sample displayed a

lower water retention capacity than I_A (except at saturation) because of its higher sand content (Aldana et al., 2021).

As already pointed out by Aldana et al. (2021), the hydraulic properties of the hard limestone rock samples were highly heterogeneous (**Figure 3d**). Their θ_s values were the lowest of all the VZ materials, except for the upstream weathered rock sample (R_A) which showed a coarse secondary porosity resulting in a strong decrease of θ between saturation and pF 1.0. Their θ_s values were also in good agreement with those obtained by other authors in a study conducted nearby (Legchenko et al., 2020). The massive rock samples R_B and R_C displayed a nearly constant θ between saturation and pF 3.0 in contrast to the downstream weathered rock samples (R_E and R_F), whose water retention decreased gradually over the same pF range. Compared to the weathered rock (R_A, R_E and R_F), the K values of the massive rock samples (R_B, R_C and R_D) were at first much lower near saturation (pF < 1.5) then quite close between pF 2.0 and 3.0.

3.1.2. Hydrodynamic parameters fitted by the models

The hydrodynamic parameters fitted with the DBM model using the RETC software provided the most satisfactory description of the experimental water retention and hydraulic conductivity data for all the VZ samples (**Figure 3**) compared to those obtained with the MVG (**Figure B.1**) and BBC (**Figure B.2**) models. Indeed, R² ($\geq$ 0.938) and AICc ($\leq$ -104.1) values calculated with the DBM model for each sample were always higher and lower than those obtained with the MVG (except R² for R_C and R_E) and BBC (except R² for R_E) models, respectively (**Table 2**, **Table A.1** and **Table A.2**). θ_r values were frequently set to 0 by the RETC software during the fitting procedure (**Table 2**, **Table A.1** and **Table A.2**). Some high values of correlations (> 90%) have occasionally been noted between K_s et α during the fitting made with the MVG and BBC models and between K_s, α_1 and n_1 and α_2 and n_2 for the DBM model (**Table 2**, **Table A.1** and **Table A.2**). As a reminder, when a correlation higher than 90% was noted between

two fitted parameters, the value of one of them was set to that obtained during the first fitting round and a second round was implemented.

The quality of the description of the water retention curves was more impacted by the choice of the analytical model than the hydraulic conductivity curves. The experimental water retention properties of the soft VZ materials, that mostly displayed a clear bimodal behavior (notably S_A, S_B, P_A, P_D, I_A and I_B), were poorly depicted by the MVG and BBC models, especially for $0.5 < pF < 1.5$ where retention was overestimated by the models and for $2.5 < pF < 4.0$ where it was underestimated (**Figure B.1a-c** and **Figure B.2a-c**). Higher values of parameter θ_s were obtained with the MVG (**Table A.1**) and BBC (**Table A.2**) models for a majority of the soft VZ samples (expect S_A and S_B for MVG and I_B for MVG and BBC) compared to those fitted with the DBM model (**Table 2**). The experimental hydraulic conductivity curves of all the VZ samples were generally well described by the three models which gave good fits for $1.5 < pF < 3.0$ (**Figure 3**, **Figure B.1** and **Figure B.2**). The main differences in the fitted *K(h)* curves among the three models were found in the description of the hydraulic conductivity near saturation ($pF < 1$). Indeed, the *K* values obtained by the DBM model near saturation were frequently higher or equal than those given by the MVG and BBC models (except S_C for MVG and BBC and I_A for BBC). This resulted in K_s values always higher or equal for the DBM model compared to the MVG (except P_A, I_A and R_B) and BBC (except I_A) models (**Table 2**, **Table A.1** and **Table A.2**).

The MVG and BBC models still allow a decent representation of the hydraulic properties of the VZ materials, with $R^2 \geq 0.866$ (except for S_C and R_A) and AICc $\leq$ -85.6 for MVG and $R^2 \geq 0.849$ (except for S_C and R_C) and AICc $\leq$ -75.9 for BBC (**Table A.1** and **Table A.2**). However, the quality of the fit was better for the MVG model as the AICc values computed for each sample were generally lower than those obtained for the BBC model (except for I_B and R_A). Consequently, the simulations made using the HYDRUS-1D software concerning the influence

of the choice of the analytical model on the simulation of water flow and the estimation of TT within the VZ were focused on a comparison between the unimodal (MVG) and bimodal (DBM) expressions.

Table 2: Parameters fitted with the DBM model using the RETC software and dispersivity (λ) taken from the literature for the VZ materials.

Sample (Sampling)	Lithology	Depth [m]	θ_r [cm³/cm³]	θ_s	α_1 [cm⁻¹]	n_1 [-]	K_s [cm/d]	w_2 [-]	α_2 [cm⁻¹]	n_2 [-]	R^2 [-]	AICc [-]	λ [cm]
S_A (Soil pit)	Soil	0.20	*0.000*	0.493 (0.473/0.508)	0.051 (0.046/0.057)	3.07 (2.48/3.65)	*30.24*	0.734 (0.711/0.758)	0.00042 (0.0003/0.0006)	1.27 (1.23/1.30)	0.994	-201.4	6.8
S_B (Soil pit)	Soil	0.45	*0.023*	0.471 (0.448/0.495)	0.055 (0.046/0.064)	2.62 (2.01/3.23)	*53.57*	0.734 (0.698/0.770)	0.00036 (0.0002/0.0005)	1.35 (1.28/1.42)	0.985	-185.7	6.8
S_C (Soil pit)	Soil	0.75	0.034 (0.014/0.054)	0.441 (0.428/0.453)	*0.110* *(0.080/0.140)*	*1.15*	*47.52*	0.748 (0.687/0.809)	0.00028 (0.0001/0.0004)	1.73 (1.42/2.03)	0.984	-213.6	6.8
P_A (B1)	CPL	1.15	0.045 (0.020/0.070)	0.422 (0.397/0.447)	0.046 (0.034/0.058)	1.61 (1.18/2.03)	*3.24*	0.725 (0.623/0.826)	0.00008 (0.0001/0.0001)	3.45 (2.21/4.69)	0.973	-162.3	1.6
P_B (B2)	Powdery Limestone	1.30	*0.000*	0.349 (0.338/0.360)	0.017 (0.007/0.027)	1.21 (1.15/1.28)	*0.95*	0.590 (0.451/0.723)	0.00012 (0.0001/0.0002)	*2.16*	0.951	-115.0	1.6
P_C (B1)	Powdery Limestone	5.00	*0.000*	0.292 (0.275/0.308)	*0.0095*	1.41 (1.17/1.66)	*0.15*	0.817 (0.697/0.937)	0.00015 (-0.0001/0.0004)	1.40 (1.13/1.67)	0.940	-110.4	1.6
P_D (B2)	Powdery Limestone	6.35	*0.000*	0.338 (0.327/0.349)	*0.051*	1.18 (1.13/1.22)	6.42	0.800 (0.743/0.858)	0.00007 (0.0000/0.0001)	1.92 (1.52/2.33)	0.976	-155.8	1.6
I_A (B2)	Calcareous Sand	3.80	0.012 (-0.023/0.048)	0.362 (0.333/0.391)	0.063 (0.057/0.073)	1.62 (1.35/1.89)	*10.98*	0.660 (0.494/0.826)	0.00009 (0.0001/0.0001)	*2.86*	0.985	-104.1	5.9
I_B (B3)	Calcareous Sand	4.25	*0.000*	0.434 (0.407/0.461)	0.185 (0.165/0.206)	*4.69*	285	0.484 (0.446/0.523)	0.0043 (0.0011/0.0076)	1.31 (1.22/1.40)	0.978	-144.1	5.9
R_A (B2)	UW Rock	5.20	*0.000*	0.340 (0.319/0.361)	0.242 (0.137/0.347)	6.39 (1.55/11.23)	*5000*	0.294 (0.238/0.349)	0.0242 (-0.0138/0.0621)	1.19 (1.11/1.28)	0.974	-154.7	0.2
R_B (B2)	Massive Rock	6.85	*0.000*	0.147 (0.139/0.155)	0.021 (0.018/0.025)	1.37 (1.18/1.56)	*1.11*	0.691 (0.530/0.851)	*0.00001*	2.22 (1.21/3.22)	0.982	-152.0	0.2
R_C (B2)	Massive Rock	11.25	*0.000*	0.050 (0.048/0.052)	*0.032*	2.38 (1.37/3.39)	*0.016*	0.963 (0.950/0.977)	0.00036 (0.0001/0.0006)	1.32 (1.23/1.41)	0.938	-180.2	0.2
R_D (B1)	Massive Rock	13.95	0.013 (0.001/0.025)	0.114 (0.104/0.125)	1.793 (1.184/2.403)	*1.15*	*4000*	0.405 (0.231/0.579)	0.0011 (0.0004/0.0018)	2.56 (-0.08/5.19)	0.939	-153.9	0.2
R_E (B2)	DW Rock	14.60	*0.000*	0.128 (0.111/0.145)	0.641 (0.272/1.01)	*1.25*	*5000*	0.409 (0.223/0.588)	0.00085 (-0.0016/0.0033)	1.33 (0.83/1.83)	0.941	-138.0	0.2
R_F (B2)	DW Rock	16.15	*0.000*	0.161 (1.456/0.176)	0.942 (0.579/1.305)	*1.34*	*10000*	0.449 (0.342/0.556)	0.0016 (-0.0005/0.0036)	1.38 (1.11/1.65)	0.982	-142.5	0.2

Parameters highlighted in italics were fixed during the fitting procedure. Confidence intervals associated with parameters fitted using RETC are given in parentheses. CPL: cryoturbated powdery limestone, UW: upstream weathered, DW: downstream weathered.
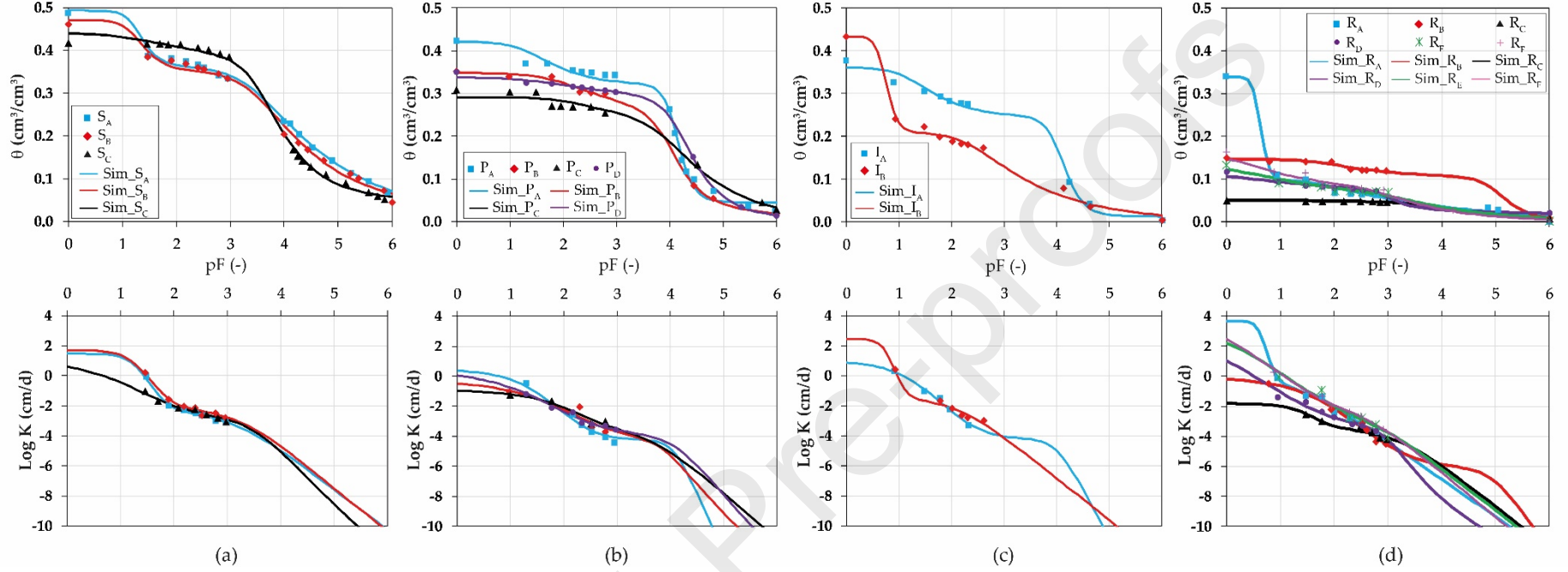
Figure 3: Comparison between experimental and fitted (DBM model) water retention ($\theta(h)$, up) and hydraulic conductivity ($K(h)$, down) curves for the soil (a), powdery limestone (b), calcareous sand (c) and limestone rock (d) samples.
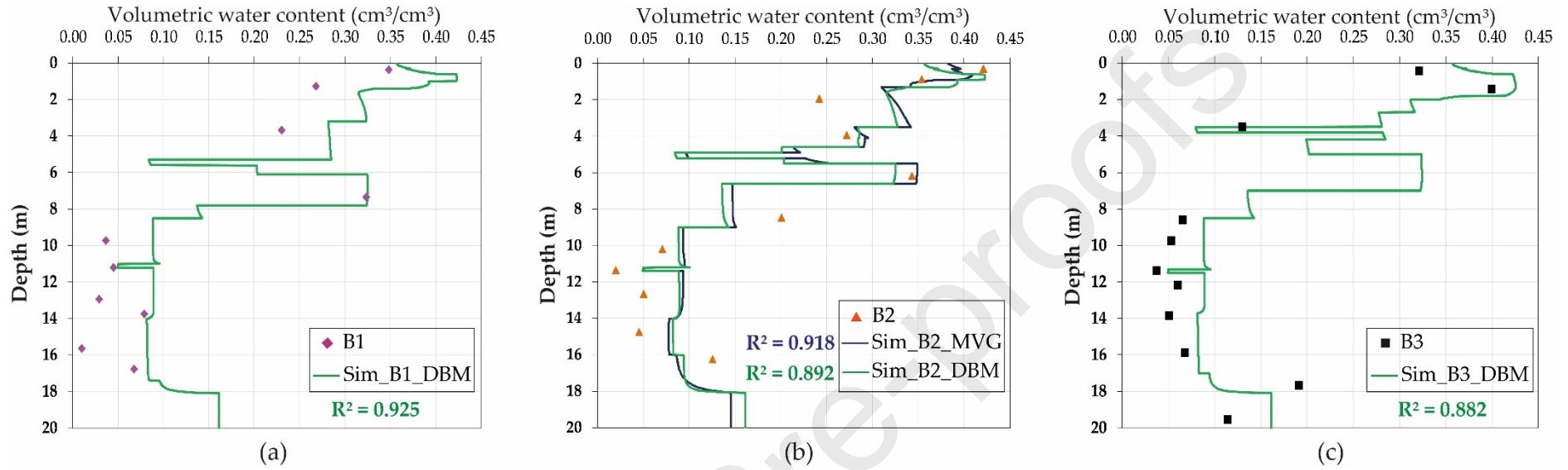
Figure 4: Comparison between measured water content profiles for B1 (a), B2 (b) and B3 (c) at the date of the drilling (14 March 2017) and those simulated by the models (DBM for B1 and B3 and MVG and DBM for B2).
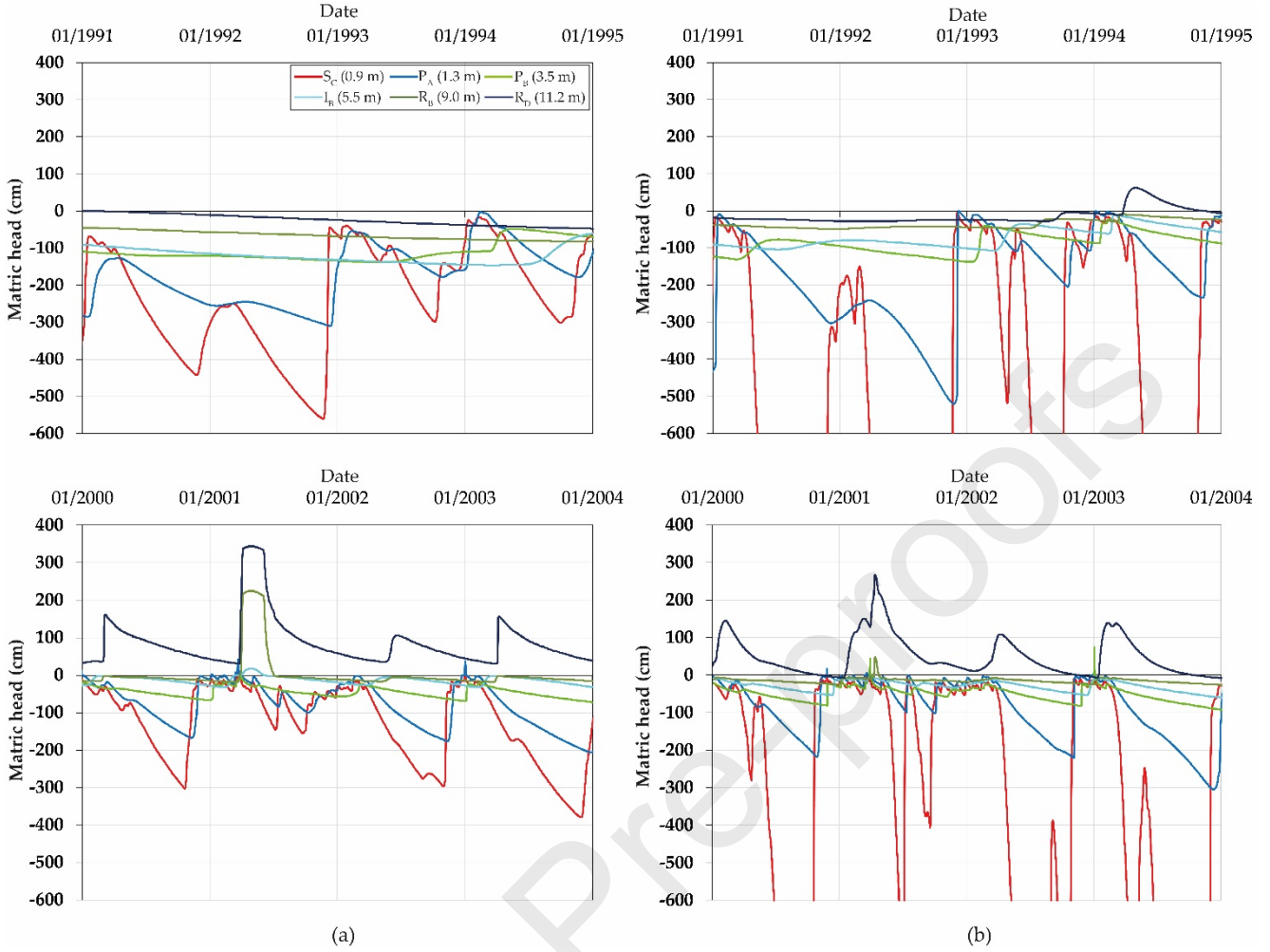
Figure 5: Simulated values of matric head obtained between 1991 and 1994 (dry VZ profile with WTL_{MIN} = -22.21 m on 19/08/1992, up) and between 2000 and 2003 (wet VZ profile with WTL_{MAX} = -14.60 m on 15/05/2001, down) at the observation nodes defined for the B2 profile (**Table 1**) with the MVG (a) and DBM (b) models.
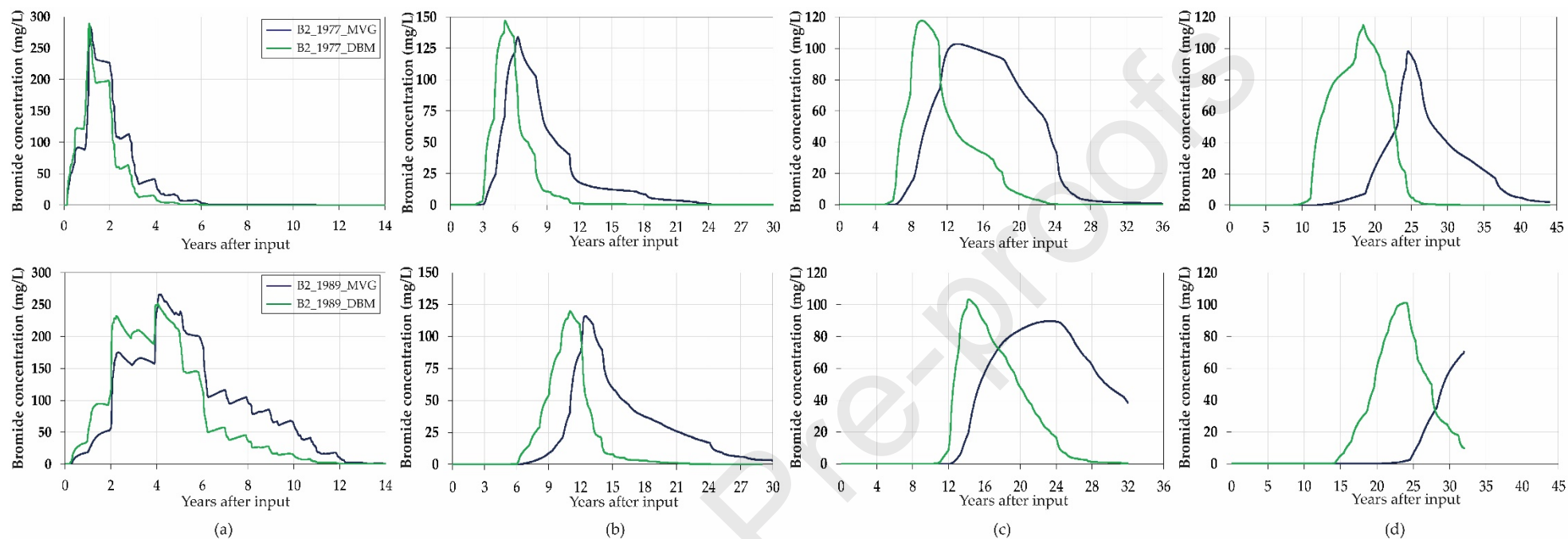
Figure 6: Bromide concentration simulated at 0.9 (a), 3.5 (b), 6.6 (c) and 14.6 m (WTL$_{MAX}$) (d) deep by the MVG and DBM models in the B2 profile and as a function of the years after input. Two input years are presented, corresponding to small (1977, up) and large (1989, down) travel time.

Table 3: Results obtained for the simulation of bromide transport down to WTL_{MAX} (-14.60 m) for the B2 profile according to the choice of the analytical model: peak concentration and mean, minimum and maximum indicators of travel time (TT_I, TT_P and TT_E).

	1968-1999		1968-1986			1968-1975	
Analytical Model	**Mean TT$_I$**	**Min TT$_I$** *Max TT$_I$*	**Peak Concentration**	**Mean TT$_P$**	**Min TT$_P$** *Max TT$_P$*	**Mean TT$_E$**	**Min TT$_E$** *Max TT$_E$*
	y	y	mg/L	y	y	y	y
MVG	18.5 (3.1)	13.1 [1974] *23.1 [1989]*	92.8 (4.0)	28.4 (3.2)	24.4 [1979] *34.9 [1986]*	44.7 (1.1)	43.4 [1974] *46.5 [1968]*
DBM	13.2 (2.1)	9.8 [1974] *16.9 [1983]*	105.9 (5.9)	18.8 (2.2)	14.6 [1974] *22.7 [1985]*	29.7 (1.7)	27.3 [1975] *32.2 [1968]*

The standard deviations associated with the peak concentration and the mean TT_I, TT_P and TT_E are given in parentheses. The years associated with the minimum and maximum TT_I, TT_P and TT_E are given in brackets.

3.2. Simulation of water flow and estimation of travel time within the B2 profile

Since a majority of the samples were taken from the B2 profile (**Table 2**), the influence of the choice of the analytical model (MVG or DBM) on the simulation of water flow and the estimation of TT within the VZ was studied on this profile.

The B2 water content profiles simulated at the date of the drilling (14 March 2017) using the MVG and DBM models were in relatively good agreement with the experimental measurements made on the undisturbed core samples on that same date ($R^2 \geq 0.892$, **Figure 4b**). The differences in θ between the two models were rather small and the main disparities (< 0.05 cm^3/cm^3) were observed within the soil (0-1 m deep), the powdery limestone facies (from 2.0 to 3.5 m deep and from 5.5 to 6.6 m deep) and the saturated zone (below 18 m deep). Overestimations of experimental θ by the models were noted in the powdery limestone material P_B (2 m deep) and in limestone rock materials (R_C, R_D and R_E) from 10 to 15 m deep. Underestimations of experimental θ by the models were observed in massive (R_B, 8.5 m deep) and downstream weathered limestone rock materials (R_F, 16 m deep).

Since the Beauce limestone aquifer is known for its highly permeable soils and its vertical soil water flow regime (Bruand et al., 1997; Flipo et al., 2012), no run off was observed during the whole simulation period (55 years and a total rainfall of 35180 mm). The matric head values simulated by the DBM model in each soil layer displayed more fluctuations than those of the MVG model (**Figure 5** and **Figure B.3**). The soil water status simulated by the DBM model was drier (lower mean values of *h*) and characterized by more pronounced drying and wetting cycles than for the MVG model (**Figure B.3** and **Table A.3**). The mean downward water flux simulated within the soil was higher for the DBM model than for the MVG model (**Table A.3**). This could be attributed to the higher cumulative ET_R (actual evapotranspiration) simulated with the MVG model (30210 mm) compared to the DBM model (28009 mm), which resulted in a lower quantity of water infiltrating in the VZ profile for the MVG model over the simulation

period. This was also induced by the higher soil K values observed near saturation (pF < 1.5) for the DBM model compared to the MVG model (except S_C) (**Figure 3a**, **Figure B.1a** and **Figure B.2a**). As a result, the bromide transport simulated within the soil by the DBM model was noticeably faster than that simulated with the MVG model (**Figure 6a**).

The mean water content and matric head values simulated by the models within the deep VZ materials (below the soil) (**Table A.3**) indicated that the DBM model resulted in a globally wetter VZ profile (higher mean values of h) compared to the MVG model. Although the variations of matric head values observed within the deep VZ materials could seem relatively close at first sight between the two models, they were in fact much more dynamic for the DBM model, as highlighted by more pronounced drying and wetting cycles (**Figure 5** and **Figure B.4**). Perched water tables were identified in the VZ profiles and were caused by the low saturated hydraulic conductivity of the powdery limestone (P_B, P_C and P_D for MVG and P_B and P_C for DBM) and massive limestone rock (R_C) (**Figure 3b,d**, **Figure B.1b,d**, **Figure 5** and **Figure B.4**). Although these perched water tables seemed slightly more pronounced for the MVG model, these were actually less frequent than for the DBM model due to the higher K near saturation (pF < 1) of the powdery limestone and rock materials and the more dynamic water regime of the latter. In accordance with the lower mean downward water flux simulated along the VZ profile (**Table A.3**), the bromide transport simulated with the MVG model from the base of the soil down to WTL_{MAX} (14.6 m deep) was always slower than that simulated with the DBM model (**Figure 6b-d**).

Finally, the mean TT_I, TT_P and TT_E (calculated from all the TT values simulated for each input year over the same period of time) were always higher for the MVG model than for the DBM model whatever the period of time considered (**Table 3**). The differences in mean TT values between the DBM and MVG models were significant and higher than 5 years for TT_I, 9 years for TT_P and 14 years for TT_E (**Table 3**). The year of input corresponding to the minimum and

maximum TT_I, TT_P and TT_E were relatively close between the two models (**Figure B.5** and **Table 3**). The most significant variations in TT simulated between the two models were noted for the years of input corresponding to a sudden increase in TT for the MVG model and which was not reproduced by the DBM model (e.g., 1978 and 1988 for TT_I; 1981 and 1982 for TT_P) (**Figure B.5**).

The simulation of the water flow and the estimation of the TT made using unimodal (MVG) and bimodal (DBM) models fitted to the same experimental hydraulic properties can show large disparities ($9.8 \leq TT_I \leq 23.1$ years, $14.6 \leq TT_P \leq 34.9$ years, $27.3 \leq TT_E \leq 46.5$ years). The DBM model allows to better account for the impact of the macroporosity in the soft VZ materials and the presence of (micro-) fissures (< 1 mm thick) in the hard limestone rock materials compared to the MVG model. In view of all these findings and since the hydrodynamic parameters fitted with the DBM model provided the most satisfactory description of the experimental hydraulic properties, the latter has been adopted for the comparative simulation of water flow and TT performed between three VZ profiles reconstituted with HYDRUS-1D from the three boreholes (B1, B2 and B3).

3.3. Simulation of the water flow and estimation of travel time within the vadose zone (B1, B2 and B3 profiles)

3.3.1. Impact of the heterogeneity of the vadose zone profiles

Simulated θ profiles with the DBM model at the date of the drilling (14/03/2017) for the three boreholes were in good agreement with the experimental measurements made on the undisturbed core samples on that same date ($0.882 \leq R^2 \leq 0.925$, **Figure 4**). Experimental θ obtained for the three boreholes were generally slightly overestimated by the model, notably in P_B and P_C materials (from 1.5 to 4.0 m deep, depending on the borehole) and in limestone rock materials from 9.0 to 16.0 m deep. The main differences between experimental and simulated

31

θ (from 0.05 to 0.10 cm^3/cm^3) within the three boreholes were found (i) in S_B, P_A and P_B materials above 2.0 m deep; (ii) in R_B materials around 8.0 m deep, at the transition between the powdery limestone (P_D) and the massive rock (R_B) materials (Aldana et al., 2021), which displayed high and low θ_s values respectively (**Table 2**); (iii) in R_E and R_F materials between 15.5 and 18.0 m deep, which corresponds to the weathered limestone rock that presented a highly heterogeneous structure with an increasing evolution toward karstification, fracturation and even silicification with depth (Mallet et al., 2022).

The water regime within the soil seemed to be all the more dynamic as its thickness was small, as highlighted by the variations of the matric head, which suggested more pronounced drying and wetting cycles in the B2 profile than in B1 and B3 profiles (**Figure 7a**). The mean values of water content, matric head and water flux simulated for the three boreholes (**Table A.4**) indicated that the soil of the B3 profile was slightly wetter. It also displayed a lower vertical downward water flux than B1 and B2 profiles, although the three soil profiles were strictly identical down to 0.9 m deep (**Table 1**). This was attributed to the higher cumulative ET_R simulated within the B3 profile (28296 mm), due to the larger thickness of its soil layer S_C (1.2 m, cf. **Table 1**) compared to B1 (0.4 m) and B2 (0.3 m). Indeed, the soil showed the highest water retention capacity among the VZ materials (**Figure 3**). This resulted in a visible differentiation of the bromide transport between the B3 and the B2 and B1 profiles with a slightly slower leaching of bromide down to 1.2 m deep in the B3 soil profile (**Figure 8a**). The differences in soil profiles and the influence of the meteorological conditions led to an arrival time for the peak of bromide ranging from 1.3 to 5.1 years at 1.2 m deep (**Figure 8a**), which represented a travel speed ranging from 0.23 to 0.94 m/yr.

The mean h values simulated by the DBM model in the VZ materials below 2.0 m deep for the three boreholes were higher than -100 cm (pF < 2.0) (**Table A.4**). This revealed a global wet water status over the simulation period (**Figure 7b-d**) and the occurrence of relatively high

vertical downward water flux (due to K values close to saturation) within the VZ profiles (**Table A.4**). The strong lithological similarities between the B1 and B2 profiles down to 3.5 m deep (**Table 1**) led to a comparable bromide transport within the soil and the upper powdery limestone materials (P_A, P_B and P_C) of the two profiles (**Figure 8a-b**). The differentiation in bromide transport simulated between the B1 (the slowest) and B2 (the fastest) profiles from 3.5 m to 8.0 m deep (**Figure 8b-d**) was mainly caused by the differences in thickness of the powdery limestone materials P_C and P_D (3.8 m for B1 and 1.6 m for B2, cf. **Table 1**). The arrival time for the peak of bromide at 3.5 m and 8.0 m deep ranged from 5.0 to 11.0 years (**Figure 8b**) and from 11.1 to 18.8 years (**Figure 8c**), respectively. The peak concentration of bromide took between 3.8 and 5.9 years to migrate from 1.2 to 3.5 m deep (travel speed ranging from 0.39 to 0.63 m/yr) and between 5.0 and 7.8 years to migrate from 3.5 to 8.0 m deep (travel speed ranging from 0.58 to 0.89 m/yr).

The mean bromide peak concentration observed at WTL_{MAX} for each VZ profile was between 94.4 (B3) and 104.8 mg/L (B2) (**Table 4**) which approximately represents 1% of the bromide input concentration (9.7 g/L). The lowest peak concentrations observed for B3 were caused by the higher global dispersivity of the profile (thicker soil and thinner powdery limestone, cf. **Table 1** and **Table 2**). The highest peak concentrations found for B2 profile were induced by its lower global dispersivity (thinner soil and thicker rock materials, cf. **Table 1** and **Table 2**). It is worth noting that the higher global dispersivity of the B3 profile resulted in the observation of bromide first concentrations at WTL_{MAX} (TT_I) at times close to B2 and the total exit of the bromide (TT_E) at times close to B1 (**Figure B.6** and **Table 4**). The mean indicators of TT for bromide to reach WTL_{MAX} (14.6 m deep) were of 13.8 years for TT_I ($9.8 \leq TT_I \leq 17.5$ years), 20.9 years for TT_P ($14.6 \leq TT_P \leq 25.3$ years) and 31.5 years for TT_E ($26.6 \leq TT_P \leq 39.0$ years) (**Table 4**). The peak concentration of bromide was transported from the soil surface down to WTL_{MAX} at a mean travel speed of 0.70 m/yr (min.: 0.58 m/yr and max.: 1.00 m/yr) and took

between 5.8 to 8.3 years to migrate through the limestone rock facies from 8.0 m deep down to WTL_{MAX} (travel speed ranging from 0.79 to 1.15 m/yr) (**Figure 8d**). For a given year of input, TT_I and TT_P were always the largest for the B1 profile and the smallest for the B2 profile and TT_E was always the largest for the B3 profile and the smallest for the B2 profile (**Figure B.6**). Differences of up to 3.6 (B1-B2, 1979), 3.5 (B1-B2, 1975) and 4.7 years (B3-B2; 1977) were observed regarding TT_I, TT_P and TT_E respectively (**Figure B.6**). The impact of the lateral variations in the VZ profiles (lithological differences at small scale: less than 15 m, cf. **Figure 1**) on the variations of the TT was relatively small. This is a consequence of the overall wet status observed over the simulation period within the VZ materials located below the soil (**Figure 7b-d** and **Table A.4**) which induced a leaching of bromide mainly impacted by K values close to saturation.

3.3.2. Impact of the meteorological conditions

As previously underlined by some authors (Sprenger et al., 2016; Vero et al., 2014), meteorological conditions have a strong influence on the variation of TT through the VZ. Maximum differences in the TT indicators according to input years for each VZ profile varied from 7.0 (B1) to 7.2 (B3) years for TT_I, from 8.2 (B1) to 9.5 (B3) years for TT_P and from 7.4 (B2) to 9.7 (B3) years for TT_E (**Table 4**). The variations of the TT observed within a single VZ profile over the simulation period were higher than those observed between the three VZ profiles for a given year of input (**Figure B.6** and **Table 4**). It appeared that, in the case of a globally wet VZ, the meteorological conditions had more influence on the variations of the TT within the VZ than the small scale lateral variations of its profile lithological composition. Positive values of matric head were noted in several VZ materials located above the least permeable materials (P_B, P_C and R_C) (**Figure 3b,d** and **Figure 7b-c**), and appeared in years showing annual R-ETP balance close or above 0 mm (such as 1978-1984, 1988 or 2001-2002, cf. **Figure 2**). This indicates that perched water tables may have occurred in the VZ profiles,

caused by accumulation of water above these weakly permeable materials. The building up of perched water tables were highlighted in the soft VZ materials up to a depth of 0.7 m and in the limestone rock from about 11 m deep up to a depth of 7 m (**Figure 7c-d** and **Figure B.4b**). Given the high lithological heterogeneity of the VZ materials, these perched water tables will however probably be less significant at the 3D field scale because of the lateral movement of water into open fractures or karst networks situated within the VZ (Aldana et al., 2021; Mallet et al., 2022).

The TT variations were tightly correlated with meteorological conditions and water table level data that were used as boundary conditions over the simulation period. The relatively slow leaching of bromide observed in the VZ (mean travel speed: 0.70 m/yr) could be partly explained by the low mean annual rainfall (639.6 mm) and the high mean annual ETP (813.7 mm) observed over the simulation period (**Figure 2**) and also by the low hydraulic conductivity (even near saturation) of the powdery limestone (P_B, P_C and P_D) and the massive rock (R_B and R_C) materials (**Figure 3b,d**). The relatively faster leaching of bromide (corresponding to low TT) observed for inputs made between 1968 and 1975 (**Figure B.6**) could be explained by the meteorological conditions observed between 1977 and 1984, when annual R-ETP balances were close or above 0 mm and when WTL was rising (**Figure 2**). The global slowdown of the leaching of bromide (corresponding to a general increase in TT) observed for inputs made from the late 1970s (**Figure B.6**) was strongly influenced by the small annual rainfall and the lowering of the WTL observed from 1989 to 1998, 2003 to 2011 and 2015 to 2020 (**Figure 2**) and may be a consequence of global warming. Indeed, it is worth noting that from 1989 to 2020, only two years of input showed a positive annual R-ETP balance (1999 and 2001) while an increase in mean annual temperature (of 1.0°C) and ETP (of 98 mm) was noted compared to the 1968-1988 period (**Figure 2**). As highlighted by the trends observed for TT_I since the end of the 1990s (**Figure B.6**), a further increase in TT for inputs made after

2000 is expected as a response to the global increase in mean annual temperature and ETP observed since 2015 (maximum of 12.8°C and 1044 mm observed in 2020), associated with a strongly negative annual R-ETP balance (**Figure 2**).
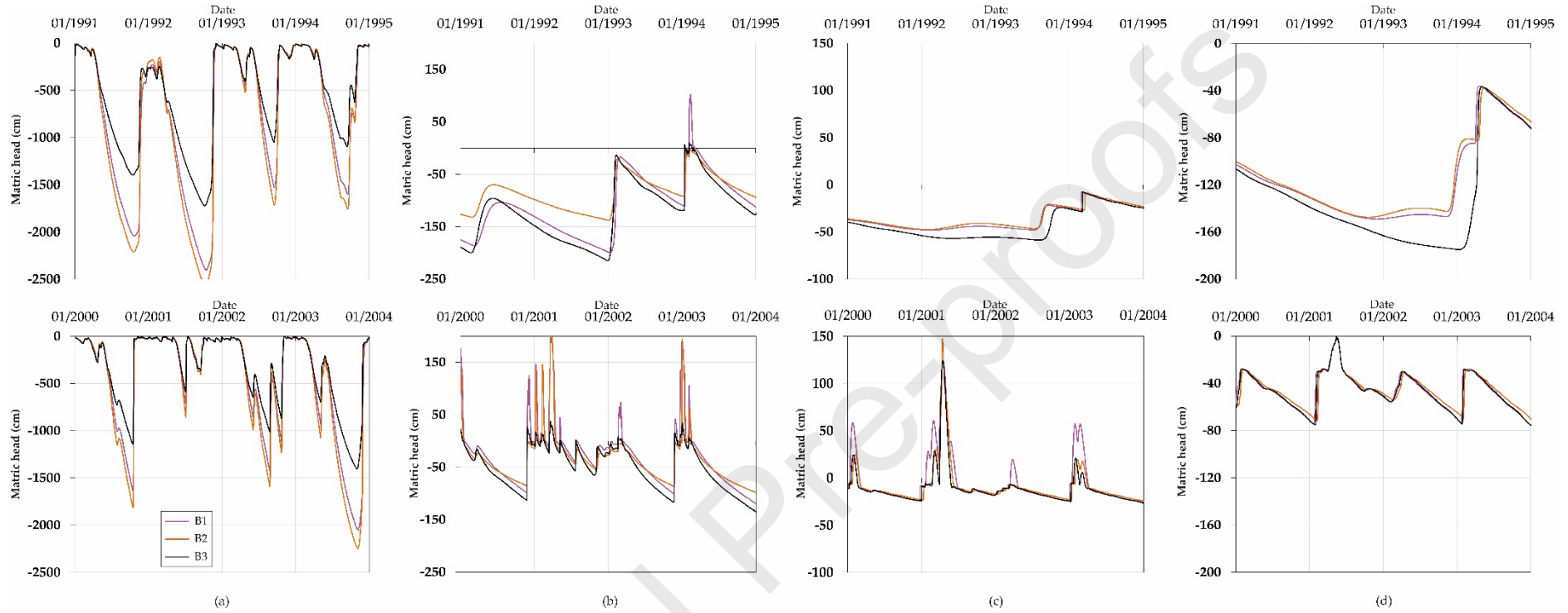
Figure 7: Simulated values of matric head obtained between 1991 and 1994 (dry VZ profile with WTL_{MIN} = -22.21 m on 19/08/1992, up) and between 2000 and 2003 (wet VZ profile with WTL_{MAX} = -14.60 m on 15/05/2001, down) at 0.9 (a), 3.3 (b), 10.0 (c) and 14.6 (d) m deep within the B1, B2 and B3 profiles with the DBM model.

Table 4: Results obtained for the bromide transport simulated down to WTL_{MAX} (-14.60 m) by the DBM model for each VZ profile (B1, B2 and B3): peak concentration and mean, minimum and maximum indicators of travel time (TT_I, TT_P and TT_E).

1968-2001	1968-1998	1968-1982

Profile	Mean TT_I	Min TT_I / Max TT_I	Peak Concentration	Mean TT_P	Min TT_P / Max TT_P	Mean TT_E	Min TT_E / Max TT_E
	y	y	mg/L	y	y	y	y
B1	14.4 (2.0)	10.5 [1978] / *17.5 [1983]*	97.4 (4.8)	21.7 (2.4)	17.1 [1972] / *25.3 [1988]*	31.9 (2.6)	28.5 [1975] / *38.2 [1982]*
B2	13.3 (2.1)	9.8 [1974] / *16.9 [1983]*	104.8 (5.1)	20.0 (2.4)	14.6 [1974] / *23.9 [1988]*	29.9 (2.3)	26.6 [1977] / *34.0 [1982]*
B3	13.7 (2.1)	9.9 [1976] / *17.1 [1983]*	94.4 (4.1)	21.0 (2.6)	15.7 [1973] / *25.2 [1988]*	32.6 (2.6)	29.3 [1974] / *39.0 [1982]*
B1-B2-B3	13.8 (2.1)	9.8 [1974 - B2] / *17.5 [1983 - B1]*	99.2 (6.6)	20.9 (2.5)	14.6 [1974 - B2] / *25.3 [1988 - B1]*	31.5 (2.8)	26.6 [1977 - B2] / *39.0 [1982 - B3]*

The standard deviations associated with the peak concentration and the mean TT_I, TT_P and TT_E are given in parentheses. The years associated with the minimum and maximum TT_I, TT_P and TT_E are given in brackets.
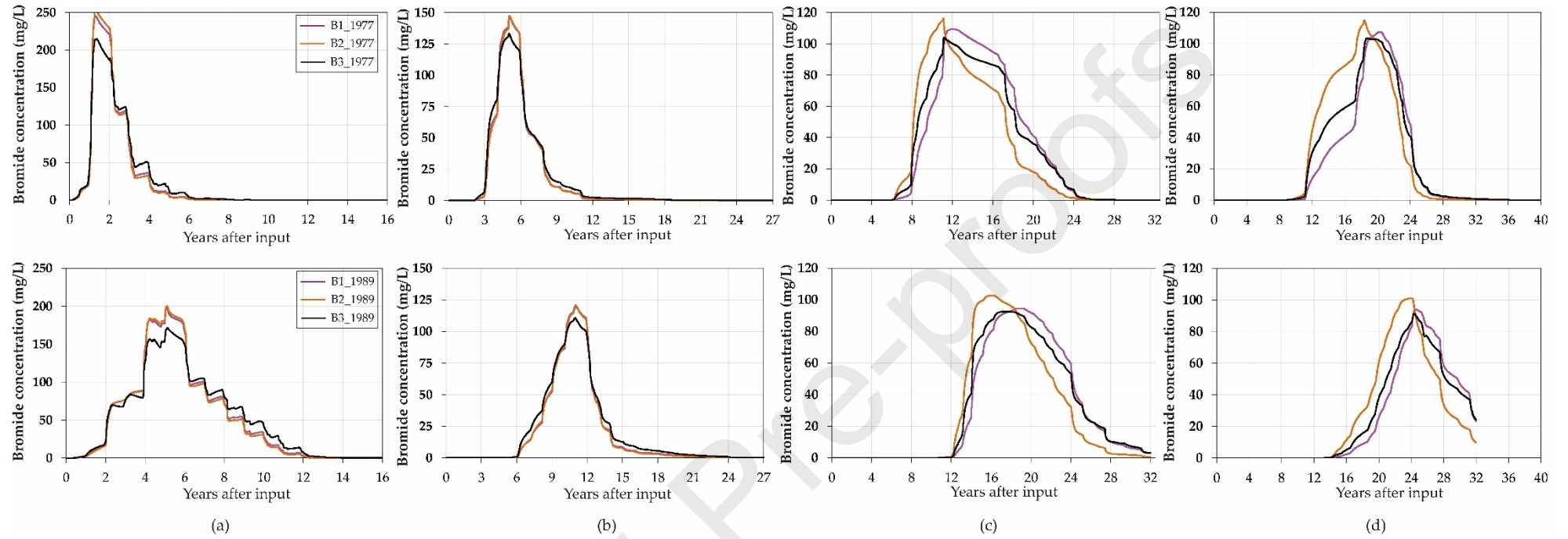
Figure 8: Bromide concentration simulated at 1.2 (a), 3.5 (b), 8.0 (c) and 14.6 m (WTL$_{MAX}$) (d) deep by the DBM model in the three VZ profiles

(B1, B2 and B3) as a function of the years after input. Two input years are presented, corresponding to small (1977, up) and large travel time (1989,

down).

3.4. Limitation of the work

The results obtained and discussed in this study focused on the simulation of the movement of water and bromide in the VZ of the Beauce limestone aquifer at the core scale. It has been well established that interconnected fractures or karst networks may act as preferential flow paths leading to faster water and solute transport (Chen et al., 2019; McLing et al., 2017; Wood et al., 2004), notably after heavy rainfall events and thus only under or close to fully saturated conditions (Wellings and Bell, 1980). Some authors suggested that several tens of percent of the total flow in the VZ could be transported through fractures (Smith et al., 1970). As shown on **Figure 9**, natural fractures with karstification were observed at the field scale and were found to have been episodically subjected to intense water flow, under or close to fully saturated conditions (Aldana et al., 2021; Mallet et al., 2022).
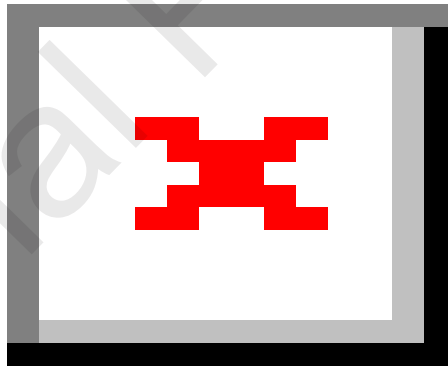

Figure 9: Optical imaging of five new boreholes (B5, B6, B7, B8 and B9 drilled in Spring 2020 at a few tens meters from B1, B2 and B3) highlighting fractures and karstification processes observed between 12.6 and 13.5 m deep in the rock formation of the Beauce limestone aquifer.

The simulations carried out in this work showed the possible occurrence of perched water tables within the VZ which might generate preferential water flow through these open fractures networks, especially in the case of very rainy years. This would result in a faster solute transport within the fracture porosity which could be simulated by the use of a dual permeability model (Šimůnek et al., 2003). This modeling approach has proven to be useful for taking into account the contribution of preferential flow and representing the water flow and solute transport between fractures and matrix (Aguilar-López et al., 2020; Köhne et al., 2002). Recent work also showed that, even if a dual-porosity model was capable of adequately describing the arrival of the measured initial concentrations and the shape of the breakthrough curves of bromide at the base of a loamy soil, only the dual permeability model used with the inclusion of a mobile-immobile water component (MIM) provided a good ability to identify the arrival of peak concentrations (Varvaris et al., 2021b). The identification and characterization of these open fractures networks and the understanding of their functioning will consequently be crucial for complementing our knowledge of water flow, travel time and contaminant transport through the vulnerable Beauce limestone aquifer.

Summary and Conclusion

In this study, the numerical simulation of water flow and the estimation of water travel time through the highly heterogeneous VZ of a limestone aquifer was undertaken over a period of 55 years. The parameterization of the model (HYDRUS-1D) was based on hydraulic properties laboratory measurements performed on fifteen samples representative of the lithologies encountered within the VZ using unimodal (MVG) and bimodal (DBM) approaches. Three heterogeneous VZ profiles were reconstituted in HYDRUS-1D based on three boreholes drilled in March 2017. Daily rainfall, ETP and water table level data were used as inputs for the implementation of a virtual bromide tracing experiment made over the 55 years. The arrival time of the initial breakthrough (TT_I), the peak (TT_P) and the total exit of the bromide

concentration (TT_E) at the maximum water table level were considered as suitable indicators of water travel time within the VZ of the Beauce limestone aquifer.

The results obtained in this work highlighted that the experimental hydraulic properties of the samples were more accurately described by the DBM model. The latter allowed a precise description of the bimodal characteristic of the VZ materials, i.e., macro- and micro-porosity for the soil, powdery limestone and calcareous sand samples, and matrix and (micro-)fissures porosity for the limestone rock. The choice of the analytical model used to describe the VZ hydraulic properties (MVG or DBM) showed a significant influence on the simulation of the water flow and TT within the VZ. The results of the simulations carried out with the two models displayed strong discrepancies regarding the water flow dynamics (matric head and water content variations) through the VZ and showed large differences in TT (occasionally higher than 10 years for TT_I and TT_P and 15 years for TT_E). These disparities were mainly attributed to the differences observed in the water flow dynamics simulated in the soil and the higher hydraulic conductivity values obtained with the DBM model for the VZ materials located below the soil over the range of matric head ($h > -250$ cm) observed during the simulation period.

A mean TT_I of 13.8 years (min. 9.8 – max. 17.5), TT_P of 20.9 years (min 14.6 – max. 25.3) and TT_E of 31.5 years (min 26.6 – max. 39.0) were found for the VZ of the Beauce limestone aquifer with simulations carried out using the DBM model. The vertical heterogeneity of the properties of the VZ materials showed a strong influence on the simulation of the water flow and the estimation of TT. Significant differences were found in the travel speed of the peak concentrations of bromide through the VZ materials, which was the fastest in the limestone rock facies (max. of 1.15 m/yr) and the slowest in the powdery limestone facies (max. of 0.63 m/yr). Despite the lithological differences observed between the three VZ profiles, only slight variations were found regarding the water flow dynamics and the TT (max. 4.7 years whatever the indicator) between the three boreholes. This small impact of the lateral

heterogeneities was mainly attributed to the global wet status found in the VZ materials located below the soil, which led to hydraulic conductivities always close to saturation and consequently hardly noticeable differences between the three VZ profiles. The meteorological conditions have shown a large influence on the variations of the TT through the VZ (max. 9.7 years whatever the indicator). Together with the rise of the mean annual temperature and ETP over the simulation period, an increase in TT was noted since the late 1970s, becoming even more apparent after the late 1990s and may be a consequence of global warming. In the case of this mostly unconfined aquifer, this could mean that the impact of the regulatory measures that have been put into effect since the beginning of the 1990s (e.g., the Nitrates Directive, European Commission, 1991) for the preservation of groundwater resources may not yet be clearly identifiable today and that it could take progressively longer to identify such impacts in the future.

The results presented in this work were obtained with fifteen samples selected along the whole VZ profile, and represent a first step towards capturing and deciphering in depth the high heterogeneity of the VZ materials and characterizing the complexity of the transfer through the VZ of the Beauce limestone aquifer (Aldana et al., 2021; Mallet et al., 2022). It will indeed be necessary to improve our knowledge about the vertical and lateral flow of water and solute through the whole porosity of this highly heterogeneous VZ, by conducting extensive studies at larger scales, combining 3D experimental observations and numerical simulations with dual permeability approaches. To this end, noninvasive hydrogeophysical monitoring tools seem to represent a worthwhile solution for mapping geological facies properties and linking measured geophysical parameters to the hydraulic properties of the VZ materials (Binley et al., 2015; Parsekian et al., 2015; Romero-Ruiz et al., 2018). When combined with the use of well-established or advanced *in situ* methods in the VZ (i.e., tracer tests and fracture networks characterization) (McLing et al., 2017; Sprenger et al., 2016) or in the saturated zone (pumping,

slug or tracer tests) (Binet et al., 2017; Mosthaf et al., 2018), such tools should lead to a refined

hydraulic characterization of the materials and a more accurate assessment of the travel time of

water and the fate of contaminants through this highly vulnerable limestone aquifer of major

importance.

Acknowledgements

References

Aguilar-López, J.P., Bogaard, T., Gerke, H.H., 2020. Dual-Permeability Model Improvements for Representation of Preferential Flow in Fractured Clays. Water Resour. Res. 56. https://doi.org/10.1029/2020WR027304

Aldana, C., Isch, A., Bruand, A., Azaroual, M., Coquet, Y., 2021. Relationship between hydraulic properties and material features in a heterogeneous vadose zone of a vulnerable limestone aquifer. Vadose Zone Journal 20, e20127. https://doi.org/10.1002/vzj2.20127

Amraoui, N., Thiéry, D., Croiset, N., Salquebre, D., 2017. Projet ESPOL : Modélisation à différentes échelles de l'écoulement et du transport dans le sol et la zone non saturée (No. BRGM/RP-67056-FR). BRGM.

Arora, B., Dwivedi, D., Faybishenko, B., Wainwright, H.M., Jana, R.B., 2019. 10. Understanding and Predicting Vadose Zone Processes, in: Druhan, J., Tournassat, C. (Eds.), Reactive Transport in Natural and Engineered Systems. De Gruyter, Berlin, Boston, pp. 303–328. https://doi.org/10.1515/9781501512001-011

Asadollahi, M., Stumpp, C., Rinaldo, A., Benettin, P., 2020. Transport and Water Age Dynamics in Soils: A Comparative Study of Spatially Integrated and Spatially Explicit Models. Water Resources Research 56, e2019WR025539. https://doi.org/10.1029/2019WR025539

Baize, D., Girard, M.C., 2009. Référentiel pédologique 2008, Savoir Faire. Quae, Versailles.

Bear, J., 1972. Dynamics of Fluids In Porous Media. American Elsevier Publishing Company, New York.

Binet, S., Joigneaux, E., Pauwels, H., Albéric, P., Fléhoc, Ch., Bruand, A., 2017. Water exchange, mixing and transient storage between a saturated karstic conduit and the surrounding aquifer: Groundwater flow modeling and inputs from stable water isotopes. Journal of Hydrology 544, 278–289. https://doi.org/10.1016/j.jhydrol.2016.11.042

Binley, A., Hubbard, S.S., Huisman, J.A., Revil, A., Robinson, D.A., Singha, K., Slater, L.D., 2015. The emergence of hydrogeophysics for improved understanding of subsurface processes over multiple scales: The Emergence of Hydrogeophysics. Water Resour. Res. 51, 3837–3866. https://doi.org/10.1002/2015WR017016

Bogena, H.R., Montzka, C., Huisman, J.A., Graf, A., Schmidt, M., Stockinger, M., Hebel, C. von, Hendricks-Franssen, H.J., Kruk, J. van der, Tappe, W., Lücke, A., Baatz, R., Bol, R., Groh, J., Pütz, T., Jakobi, J., Kunkel, R., Sorg, J., Vereecken, H., 2018. The TERENO-Rur Hydrological Observatory: A Multiscale Multi-Compartment Research Platform for the Advancement of Hydrological Science. Vadose Zone Journal 17, 180055. https://doi.org/10.2136/vzj2018.03.0055

Bouraoui, F., Grizzetti, B., 2014. Modelling mitigation options to reduce diffuse nitrogen water pollution from agriculture. Science of The Total Environment 468–469, 1267–1277. https://doi.org/10.1016/j.scitotenv.2013.07.066

Brantley, S.L., White, T., West, N., Williams, J.Z., Forsythe, B., Shapich, D., Kaye, J., Lin, H., Shi, Y., Kaye, M., Herndon, E., Davis, K.J., He, Y., Eissenstat, D., Weitzman, J., DiBiase, R., Li, L., Reed, W., Brubaker, K., Gu, X., 2018. Susquehanna Shale Hills Critical Zone Observatory: Shale Hills in the Context of Shaver's Creek Watershed. Vadose Zone Journal 17, 180092. https://doi.org/10.2136/vzj2018.04.0092

Brooks, R.H., Corey, A.T., 1966. Properties of Porous Media Affecting Fluid Flow. Journal of the Irrigation and Drainage Division 92, 61–88. https://doi.org/10.1061/JRCEA4.0000425

Brooks, R.H., Corey, A.T., 1964. Hydraulic Properties of Porous Media. Hydrology Papers 3, Colorado State University 27.

Bruand, A., Creusot, G., Quétin, P., Darthout, R., Raison, L., Courtemanche, P., Gaillard, H., 1997. Variabilité de la recharge de la nappe de Beauce: Rôle de l'irrigation et des caractéristiques du sol. Étude et Gestion des Sols Association Française pour l'Etude des Sols, 229-245

Burdine, N.T., 1953. Relative Permeability Calculations From Pore Size Distribution Data. Journal of Petroleum Technology 5, 71–78. https://doi.org/10.2118/225-G

Chen, N., Valdes, D., Marlin, C., Blanchoud, H., Guerin, R., Rouelle, M., Ribstein, P., 2019. Water, nitrate and atrazine transfer through the unsaturated zone of the Chalk aquifer in northern France. Science of The Total Environment 652, 927–938. https://doi.org/10.1016/j.scitotenv.2018.10.286

DDT, 2016. Masse d'eau souterraine FRGG092 "Calcaires tertiaires libres de Beauce." Direction départementale des territoires du Loiret. Service eau, environnement et forêt.

D'Emilio, A., Aiello, R., Consoli, S., Vanella, D., Iovino, M., 2018. Artificial Neural Networks for Predicting the Water Retention Curve of Sicilian Agricultural Soils. Water 10, 1431. https://doi.org/10.3390/w10101431

de Frutos Cachorro, J., Erdlenbruch, K., Tidball, M., 2017. A dynamic model of irrigation and land-use choice: application to the Beauce aquifer in France. European Review of Agricultural Economics 44, 99–120. https://doi.org/10.1093/erae/jbw005

Dimitrov, M., Vanderborght, J., Kostov, K.G., Jadoon, K.Z., Weihermüller, L., Jackson, T.J., Bindlish, R., Pachepsky, Y., Schwank, M., Vereecken, H., 2014. Soil Hydraulic Parameters and Surface Soil Moisture of a Tilled Bare Soil Plot Inversely Derived from L-Band Brightness Temperatures. Vadose Zone Journal 13, vzj2013.04.0075. https://doi.org/10.2136/vzj2013.04.0075

Durner, W., 1994. Hydraulic conductivity estimation for soils with heterogeneous pore structure. Water Resour. Res. 30, 211–223. https://doi.org/10.1029/93WR02676

Duval, O., Isambert, M., 1992. Notice explicative de la carte pédologique de Villamblain (Beauce) au 1/10 000e, Contrat de recherche site expérimental de Villamblain, rapport période 1991-1992, SESCPF-INRA.

European Commission, 2009. Directive 2009/128/EC of the European Parliament and of the Council of 21 October 2009 establishing a framework for Community action to achieve the sustainable use of pesticides.

European Commission, 2000. Directive 2000/60/EC of the European Parliament and of the Council of 23 October 2000 establishing a framework for Community action in the field of water policy.

European Commission, 1991. Council directive of 12 December 1991 concerning the protection of waters against pollution caused by nitrates from agricultural sources (91/676/EEC).

Feddes, R.A., Kowalik, P.J., Zaradny, H., 1978. Simulation of Field Water Use and Crop Yield. Wiley.

Fenton, O., Schulte, R.P.O., Jordan, P., Lalor, S.T.J., Richards, K.G., 2011. Time lag: a methodology for the estimation of vertical and horizontal travel and flushing timescales to nitrate threshold concentrations in Irish aquifers. Environmental Science & Policy 14, 419–431. https://doi.org/10.1016/j.envsci.2011.03.006

Fenton, O., Vero, S., Ibrahim, T.G., Murphy, P.N.C., Sherriff, S.C., Ó Huallacháin, D., 2015. Consequences of using different soil texture determination methodologies for soil physical quality and unsaturated zone time lag estimates. Journal of Contaminant Hydrology 182, 16–24. https://doi.org/10.1016/j.jconhyd.2015.07.004

Flipo, N., Monteil, C., Poulin, M., de Fouquet, C., Krimissa, M., 2012. Hybrid fitting of a hydrosystem model: Long-term insight into the Beauce aquifer functioning (France). Water Resour. Res. 48, W05509. https://doi.org/10.1029/2011WR011092

Gaillardet, J., Braud, I., Hankard, F., Anquetin, S., Bour, O., Dorfliger, N., Dreuzy, J.R. de, Galle, S., Galy, C., Gogo, S., Gourcy, L., Habets, F., Laggoun, F., Longuevergne, L., Borgne, T.L., Naaim-Bouvet, F., Nord, G., Simonneaux, V., Six, D., Tallec, T., Valentin, C., Abril, G., Allemand, P., Arènes, A., Arfib, B., Arnaud, L., Arnaud, N., Arnaud, P., Audry, S., Comte, V.B., Batiot, C., Battais, A., Bellot, H., Bernard, E., Bertrand, C., Bessière, H., Binet, S., Bodin, J., Bodin, X., Boithias, L., Bouchez, J., Boudevillain, B., Moussa, I.B., Branger, F., Braun, J.J., Brunet, P., Caceres, B., Calmels, D., Cappelaere, B., Celle-Jeanton, H., Chabaux, F., Chalikakis, K., Champollion, C., Copard, Y., Cotel, C., Davy, P., Deline, P., Delrieu, G., Demarty, J., Dessert, C., Dumont, M., Emblanch, C., Ezzahar, J., Estèves, M., Favier, V., Faucheux, M., Filizola, N., Flammarion, P., Floury, P., Fovet, O., Fournier, M., Francez, A.J., Gandois, L., Gascuel, C., Gayer, E., Genthon, C., Gérard, M.F., Gilbert, D., Gouttevin, I., Grippa, M., Gruau, G., Jardani, A., Jeanneau, L., Join, J.L., Jourde, H., Karbou, F., Labat, D., Lagadeuc, Y., Lajeunesse, E., Lastennet, R., Lavado, W., Lawin, E., Lebel, T., Bouteiller, C.L., Legout, C., Lejeune, Y., Meur, E.L., Moigne, N.L., Lions, J., Lucas, A., Malet, J.P., Marais-Sicre, C., Maréchal, J.C., Marlin, C., Martin, P., Martins, J.,

Martinez, J.M., Massei, N., Mauclerc, A., Mazzilli, N., Molénat, J., Moreira-Turcq, P., Mougin, E., Morin, S., Ngoupayou, J.N., Panthou, G., Peugeot, C., Picard, G., Pierret, M.C., Porel, G., Probst, A., Probst, J.L., Rabatel, A., Raclot, D., Ravanel, L., Rejiba, F., René, P., Ribolzi, O., Riotte, J., Rivière, A., Robain, H., Ruiz, L., Sanchez-Perez, J.M., Santini, W., Sauvage, S., Schoeneich, P., Seidel, J.L., Sekhar, M., Sengtaheuanghoung, O., Silvera, N., Steinmann, M., Soruco, A., Tallec, G., Thibert, E., Lao, D.V., Vincent, C., Viville, D., Wagnon, P., Zitouna, R., 2018. OZCAR: The French Network of Critical Zone Observatories. Vadose Zone Journal 17, 180067. https://doi.org/10.2136/vzj2018.04.0067

Galle, S., Grippa, M., Peugeot, C., Moussa, I.B., Cappelaere, B., Demarty, J., Mougin, E., Panthou, G., Adjomayi, P., Agbossou, E.K., Ba, A., Boucher, M., Cohard, J.-M., Descloitres, M., Descroix, L., Diawara, M., Dossou, M., Favreau, G., Gangneron, F., Gosset, M., Hector, B., Hiernaux, P., Issoufou, B.-A., Kergoat, L., Lawin, E., Lebel, T., Legchenko, A., Abdou, M.M., Malam-Issa, O., Mamadou, O., Nazoumou, Y., Pellarin, T., Quantin, G., Sambou, B., Seghieri, J., Séguis, L., Vandervaere, J.-P., Vischel, T., Vouillamoz, J.-M., Zannou, A., Afouda, S., Alhassane, A., Arjounin, M., Barral, H., Biron, R., Cazenave, F., Chaffard, V., Chazarin, J.-P., Guyard, H., Koné, A., Mainassara, I., Mamane, A., Oi, M., Ouani, T., Soumaguel, N., Wubda, M., Ago, E.E., Alle, I.C., Allies, A., Arpin-Pont, F., Awessou, B., Cassé, C., Charvet, G., Dardel, C., Depeyre, A., Diallo, F.B., Do, T., Fatras, C., Frappart, F., Gal, L., Gascon, T., Gibon, F., Guiro, I., Ingatan, A., Kempf, J., Kotchoni, D.O.V., Lawson, F.M.A., Leauthaud, C., Louvet, S., Mason, E., Nguyen, C.C., Perrimond, B., Pierre, C., Richard, A., Robert, E., Román-Cascón, C., Velluet, C., Wilcox, C., 2018. AMMA-CATCH, a Critical Zone Observatory in West Africa Monitoring a Region in Transition. Vadose Zone Journal 17, 180062. https://doi.org/10.2136/vzj2018.03.0062

Gardner, W.R., 1956. Calculation of Capillary Conductivity from Pressure Plate Outflow Data. Soil Science Society of America Journal 20, 317–320. https://doi.org/10.2136/sssaj1956.03615995002000030006x

Graveline, N., 2020. Combining flexible regulatory and economic instruments for agriculture water demand control under climate change in Beauce. Water Resources and Economics 29, 100143. https://doi.org/10.1016/j.wre.2019.100143

Guo, L., Lin, H., 2016. Critical Zone Research and Observatories: Current Status and Future Perspectives. Vadose Zone Journal 15, vzj2016.06.0050. https://doi.org/10.2136/vzj2016.06.0050

Haws, N.W., Rao, P.S.C., Simunek, J., Poyer, I.C., 2005. Single-porosity and dual porosity modeling of water flow and solute transport in subsurface-drained fields using effective field-scale parameters. Journal of Hydrology 313, 257–273. https://doi.org/10.1016/j.jhydrol.2005.03.035

Isch, A., Aldana, C., Coquet, Y., Azaroual, M., 2020. Material Characteristics, Hydraulic Properties, and Water Travel Time through the Heterogeneous Vadose Zone of a Cenozoic Limestone Aquifer (Beauce, France). https://doi.org/10.5194/egusphere-egu2020-5862

Isch, A., Montenach, D., Hammel, F., Ackerer, P., Coquet, Y., 2019. A Comparative Study of Water and Bromide Transport in a Bare Loam Soil Using Lysimeters and Field Plots. Water 11, 1199. https://doi.org/10.3390/w11061199

IUSS Working Group WRB, 2015. World Reference Base for Soil Resources 2014, update 2015. International soil classification system for naming soils and creating legends for soil maps. World Soil Resources Reports No. 106. FAO, Rome.

Jacques, D., Šimůnek, J., Timmerman, A., Feyen, J., 2002. Calibration of Richards' and convection–dispersion equations to field-scale water flow and solute transport under rainfall conditions. J. Hydrol. 259, 15–31.

Jensen, K.H., Refsgaard, J.C., 2018. HOBE: The Danish Hydrological Observatory. Vadose Zone Journal 17, 180059. https://doi.org/10.2136/vzj2018.03.0059

Jeong, J., Park, E., Han, W.S., Kim, K.-Y., Oh, J., Ha, K., Yoon, H., Yun, S.-T., 2017. A method of estimating sequential average unsaturated zone travel times from precipitation and water table level time series data. Journal of Hydrology 554, 570–581. https://doi.org/10.1016/j.jhydrol.2017.09.042

Ju, Y., Massoudieh, A., Kaown, D., Yoon, Y.-Y., Lee, K.-K., 2020. Characterization of flow dynamics around highly-utilized agricultural wells in a fractured-rock aquifer: Assessment of uncertainties lying on groundwater age-dating. Journal of Hydrology 586, 124885. https://doi.org/10.1016/j.jhydrol.2020.124885

Köhne, J.M., Köhne, S., Gerke, H.H., 2002. Estimating the hydraulic functions of dual permeability models from bulk soil data. Water Resources Research 38, 26-1-26–11. https://doi.org/10.1029/2001WR000492

Konikow, L.F., 2011. The Secret to Successful Solute-Transport Modeling. Groundwater 49, 144–159. https://doi.org/10.1111/j.1745-6584.2010.00764.x

Kurotori, T., Zahasky, C., Hosseinzadeh Hejazi, S.A., Shah, S.M., Benson, S.M., Pini, R., 2019. Measuring, imaging and modelling solute transport in a microporous limestone. Chemical Engineering Science 196, 366–383. https://doi.org/10.1016/j.ces.2018.11.001

Laio, F., Di Baldassarre, G., Montanari, A., 2009. Model selection techniques for the frequency analysis of hydrological extremes. Water Resour. Res. 45. https://doi.org/10.1029/2007WR006666

Le Coz, D., 2000. Gestion durable d'une ressource en eaux souterraines Cas de la nappe de Beauce. La Houille Blanche 116–121. https://doi.org/10.1051/lhb/2000085

Legchenko, A., Baltassat, J.-M., Duwig, C., Boucher, M., Girard, J.-F., Soruco, A., Beauce, A., Mathieu, F., Legout, C., Descloitres, M., Gabriela Patricia, F.A., 2020. Time-lapse magnetic resonance sounding measurements for numerical modeling of water flow in variably saturated media. Journal of Applied Geophysics 175, 103984. https://doi.org/10.1016/j.jappgeo.2020.103984

Légifrance, 1992. Loi n° 92-3 du 3 janvier 1992 sur l'eau. https://www.legifrance.gouv.fr/eli/loi/1992/1/3/ENVX9100061L/jo/texte

Leij, F.J., van Genuchten, M.T., 2002. Solute transport. In: Warrick, A.W. (Ed.), Soil Physics Companion. CRC Press, Boca Raton, FL, 297–341.

Lejars, C., Fusillier, J.L., Bouarfa, S., Coutant, C., Brunel, L., Rucheton, G., 2012. Limitation of agricultural groundwater uses in Beauce (France): what are the impacts on farms and on the food-processing sector ? Irrigation and Drainage 61, 54–64. https://doi.org/10.1002/ird.1659

Li, L., DiBiase, R.A., Vecchio, J.D., Marcon, V., Hoagland, B., Xiao, D., Wayman, C., Tang, Q., He, Y., Silverhart, P., Szink, I., Forsythe, B., Williams, J.Z., Shapich, D., Mount, G.J., Kaye, J., Guo, L., Lin, H., Eissenstat, D., Dere, A., Brubaker, K., Kaye, M., Davis, K.J., Russo, T., Brantley, S.L., 2018. The Effect of Lithology and Agriculture at the Susquehanna Shale Hills Critical Zone Observatory. Vadose Zone Journal 17, 180063. https://doi.org/10.2136/vzj2018.03.0063

Lide, D.R., 2004. CRC Handbook of Chemistry and Physics, 85th Edition. CRC Press.

Mallet, C., Isch, A., Laurent, G., Jodry, C., Azaroual, M., 2022. Integrated static and dynamic geophysical and geomechanical data for characterization of transport properties. International Journal of Rock Mechanics and Mining Sciences 153, 105050. https://doi.org/10.1016/j.ijrmms.2022.105050

Mattern, S., Vanclooster, M., 2010. Estimating travel time of recharge water through a deep vadose zone using a transfer function model. Environ Fluid Mech 10, 121–135. https://doi.org/10.1007/s10652-009-9148-1

McLing, T.L., Brandon, W., Zavata, B., Smith, R.W., Smith, C., Armstrong, T., Carpenter, M., 2017. The Application of Radon for Mapping Open Fracture Networks in a Thin Vadose Zone. Vadose Zone Journal 16. https://doi.org/10.2136/vzj2016.11.0116

Michot, D., Benderitter, Y., Dorigny, A., Nicoullaud, B., King, D., Tabbagh, A., 2003. Spatial and temporal monitoring of soil water content with an irrigated corn crop cover using surface electrical resistivity tomography. Water Resour. Res. 39. https://doi.org/10.1029/2002WR001581

Millington, R.J., Quirk, J.P., 1961. Permeability of porous solids. Trans. Faraday Soc. 57, 1200–1207. https://doi.org/10.1039/TF9615701200

Molénat, J., Raclot, D., Zitouna, R., Andrieux, P., Coulouma, G., Feurer, D., Grunberger, O., Lamachère, J.M., Bailly, J.S., Belotti, J.L., Azzez, K.B., Mechlia, N.B., Louati, M.B.Y., Biarnès, A., Blanca, Y., Carrière, D., Chaabane, H., Dagès, C., Debabria, A., Dubreuil, A., Fabre, J.C., Fages, D., Floure, C., Garnier, F., Geniez, C., Gomez, C., Hamdi, R., Huttel, O., Jacob, F., Jenhaoui, Z., Lagacherie, P., Bissonnais, Y.L., Louati, R., Louchart, X., Mekki, I., Moussa, R., Negro, S., Pépin, Y., Prévot, L., Samouelian, A., Seidel, J.L., Trotoux, G., Troiano, S., Vinatier, F., Zante, P., Zrelli, J., Albergel, J., Voltz, M., 2018. OMERE: A Long-Term Observatory of Soil and Water Resources, in Interaction with Agricultural and Land Management in Mediterranean Hilly Catchments. Vadose Zone Journal 17, 180086. https://doi.org/10.2136/vzj2018.04.0086

Monteith, J.L., 1965. Evaporation and environment. Symp. Soc. Exp. Biol. 19, 205–234.

Mosthaf, K., Brauns, B., Fjordbøge, A.S., Rohde, M.M., Kerrn-Jespersen, H., Bjerg, P.L., Binning, P.J., Broholm, M.M., 2018. Conceptualization of flow and transport in a limestone aquifer by multiple dedicated hydraulic and tracer tests. Journal of Hydrology 561, 532–546. https://doi.org/10.1016/j.jhydrol.2018.04.011

Mualem, Y., 1976. A new model for predicting the hydraulic conductivity of unsaturated porous media. Water Resour. Res. 12, 513–522. https://doi.org/10.1029/WR012i003p00513

O'Geen, A. (Toby), Safeeq, M., Wagenbrenner, J., Stacy, E., Hartsough, P., Devine, S., Tian, Z., Ferrell, R., Goulden, M., Hopmans, J.W., Bales, R., 2018. Southern Sierra Critical Zone Observatory and Kings River Experimental Watersheds: A Synthesis of Measurements, New Insights, and Future Directions. Vadose Zone Journal 17, 180081. https://doi.org/10.2136/vzj2018.04.0081

Ould Mohamed, S., Bruand, A., 1994. Morphology and origin of secondary calcite in soils from Beauce, France, in: Developments in Soil Science. Elsevier, pp. 27–36. https://doi.org/10.1016/S0166-2481(08)70395-7

Ould Mohamed, S., Bruand, A., Raison, L., Bruckler, L., Bertuzzi, P., Guillet, B., 1997. Estimating Long-Term Drainage at a Regional Scale Using a Deterministic Model. Soil Science Society of America Journal 61, 1473–1482. https://doi.org/10.2136/sssaj1997.03615995006100050027x

Parsekian, A.D., Singha, K., Minsley, B.J., Holbrook, W.S., Slater, L., 2015. Multiscale geophysical imaging of the critical zone. Reviews of Geophysics 53, 1–26. https://doi.org/10.1002/2014RG000465

Patil, N.G., Singh, S.K., 2016. Pedotransfer Functions for Estimating Soil Hydraulic Properties: A Review. Pedosphere 26, 417–430. https://doi.org/10.1016/S1002-0160(15)60054-6

Pham, H., 2019. A New Criterion for Model Selection. Mathematics 7, 1215. https://doi.org/10.3390/math7121215

Pisinaras, V., Panagopoulos, A., Herrmann, F., Bogena, H.R., Doulgeris, C., Ilias, A., Tziritis, E., Wendland, F., 2018. Hydrologic and Geochemical Research at Pinios Hydrologic

Observatory: Initial Results. Vadose Zone Journal 17, 180102. https://doi.org/10.2136/vzj2018.05.0102

Richards, L.A., 1931. Capillary conduction of liquids through porous mediums. J. Appl. Phys. 1, 318–333. https://doi.org/10.1063/1.1745010

Romero-Ruiz, A., Linde, N., Keller, T., Or, D., 2018. A Review of Geophysical Methods for Soil Structure Characterization. Rev. Geophys. 56, 672–697. https://doi.org/10.1029/2018RG000611

Schaap, M., Leij, F.J., Genuchten, M.T.V., 2001. Rosetta: A computer program for estimating soil hydraulic parameters with hierarchical pedotransfer functions. J. Hydrol. 251, 163–176. https://doi.org/10.1016/S0022-1694(01)00466-8

Schenk, H.J., Jackson, R.B., 2002. The global biogeography of roots. Ecological Monographs 72, 18. https://doi.org/10.1890/0012-9615(2002)072%5B0311:TGBOR%5D2.0.CO;2

Schnebelen, N., Ledoux, E., Bruand, A., Creuzot, G., 1999. Stratification hydrogéochimique et écoulements verticaux dans l'aquifère des calcaires de Beauce (France): Un système anthropisé à forte variabilité spatiale et temporelle. Comptes Rendus de l'Académie des Sciences - Series IIA - Earth and Planetary Science 329, 421–428. https://doi.org/10.1016/S1251-8050(00)80066-X

Schoups, G., Giesen, N.C. van de, Savenije, H.H.G., 2008. Model complexity control for hydrologic prediction. Water Resources Research 44. https://doi.org/10.1029/2008WR006836

Seyfried, M., Lohse, K., Marks, D., Flerchinger, G., Pierson, F., Holbrook, W.S., 2018. Reynolds Creek Experimental Watershed and Critical Zone Observatory. Vadose Zone Journal 17, 180129. https://doi.org/10.2136/vzj2018.07.0129

Šimůnek, J., Jarvis, N.J., van Genuchten, M.Th., Gärdenäs, A., 2003. Review and comparison of models for describing non-equilibrium and preferential flow and transport in the vadose zone. Journal of Hydrology 272, 14–35. https://doi.org/10.1016/S0022-1694(02)00252-4

Šimůnek, J., van Genuchten, M.Th., Šejna, M., 2016. Recent developments and applications of the HYDRUS computer software packages. Vadose Zone J. 15, 25. https://doi.org/10.2136/vzj2016.04.0033

Sisson, J.B., Genuchten, M.T. van, 1991. An improved analysis of gravity drainage experiments for estimating the unsaturated soil hydraulic functions. Water Resources Research 27, 569–575. https://doi.org/10.1029/91WR00184

Smith, D.B., Wearn, P.L., Richards, H.J., Rowe, P.C., 1970. Water Movement in the Unsaturated Zone of High and Low Permeability Strata by Measuring Natural Tritium. In: Isotope Hydrology 1970. IAEA, Vienna, 73-87.

Sousa, M.R., Jones, J.P., Frind, E.O., Rudolph, D.L., 2013. A simple method to assess unsaturated zone time lag in the travel time from ground surface to receptor. Journal of Contaminant Hydrology 144, 138–151. https://doi.org/10.1016/j.jconhyd.2012.10.007

Sprenger, M., Seeger, S., Blume, T., Weiler, M., 2016. Travel times in the vadose zone: Variability in space and time. Water Resour. Res. 52, 5727–5754. https://doi.org/10.1002/2015WR018077

Sprenger, M., Volkmann, T.H.M., Blume, T., Weiler, M., 2015. Estimating flow and transport parameters in the unsaturated zone with pore water stable isotopes. Hydrology and Earth System Sciences 19, 2617–2635. https://doi.org/10.5194/hess-19-2617-2015

Szymkiewicz, A., Gumuła-Kawęcka, A., Potrykus, D., Jaworska-Szulc, B., Pruszkowska-Caceres, M., Gorczewska-Langner, W., 2018. Estimation of Conservative Contaminant Travel Time through Vadose Zone Based on Transient and Steady Flow Approaches. Water 10, 1417. https://doi.org/10.3390/w10101417

Szymkiewicz, A., Savard, J., Jaworska-Szulc, B., 2019. Numerical Analysis of Recharge Rates and Contaminant Travel Time in Layered Unsaturated Soils. Water 11, 545. https://doi.org/10.3390/w11030545

Taylor, S.A., Ashcroft, G.L., 1972. Physical edaphology: the physics of irrigated and non-irrigated soils, Rev. and edited. ed. W.H. Freeman, San Francisco.

Turkeltaub, T., Jia, X., Zhu, Y., Shao, M., Binley, A., 2018. Recharge and Nitrate Transport Through the Deep Vadose Zone of the Loess Plateau: A Regional-Scale Model Investigation. Water Resour. Res. 54, 4332–4346. https://doi.org/10.1029/2017WR022190

van Genuchten, M.T., 1980. A closed-form equation for predicting the hydraulic conductivity of unsaturated soils. Soil Sci. Soc. Am. J. 44, 892–898.

van Genuchten, M.T., Leij, F.J., Yates, S.R., 1991. The RETC code for quantifying hydraulic functions of unsaturated soils. US Department of Agriculture: Riverside, CA, USA,

Vanderborght, J., Vereecken, H., 2007. Review of dispersivities for transport modeling in soils. Vadose Zone J. 6, 29–52. https://doi.org/10.2136/vzj2006.0096

Varvaris, I., Pittaki-Chrysodonta, Z., Duus Børgesen, C., Iversen, B.V., 2021a. Parameterization of two-dimensional approaches in HYDRUS-2D: Part 1. Simulating water flow dynamics at the field scale. Soil Science Society of America Journal 85, 1578–1599. https://doi.org/10.1002/saj2.20307

Varvaris, I., Pittaki-Chrysodonta, Z., Duus Børgesen, C., Iversen, B.V., 2021b. Parameterization of two-dimensional approaches in HYDRUS-2D: Part 2. Solute transport at the field and column scale. Soil Science Society of America Journal 85, 1496–1518. https://doi.org/10.1002/saj2.20262

Vereecken, H., Schnepf, A., Hopmans, J.W., Javaux, M., Or, D., Roose, T., Vanderborght, J., Young, M.H., Amelung, W., Aitkenhead, M., Allison, S.D., Assouline, S., Baveye, P., Berli, M., Brüggemann, N., Finke, P., Flury, M., Gaiser, T., Govers, G., Ghezzehei, T., Hallett, P., Franssen, H.J.H., Heppell, J., Horn, R., Huisman, J.A., Jacques, D., Jonard, F., Kollet, S., Lafolie, F., Lamorski, K., Leitner, D., McBratney, A., Minasny, B., Montzka, C., Nowak, W., Pachepsky, Y., Padarian, J., Romano, N., Roth, K., Rothfuss, Y., Rowe, E.C., Schwen, A., Šimůnek, J., Tiktak, A., Dam, J.V., Zee, S.E.A.T.M. van der, Vogel, H.J., Vrugt, J.A., Wöhling, T., Young, I.M., 2016. Modeling Soil Processes: Review, Key Challenges, and New Perspectives. Vadose Zone Journal 15, vzj2015.09.0131. https://doi.org/10.2136/vzj2015.09.0131

Vereecken, H., Weynants, M., Javaux, M., Pachepsky, Y., Schaap, M.G., Genuchten, M.Th. van, 2010. Using Pedotransfer Functions to Estimate the van Genuchten–Mualem Soil Hydraulic Properties: A Review. Vadose Zone Journal 9, 795. https://doi.org/10.2136/vzj2010.0045

Vero, S.E., Healy, M.G., Henry, T., Creamer, R.E., Ibrahim, T.G., Richards, K.G., Mellander, P.-E., McDonald, N.T., Fenton, O., 2017. A framework for determining unsaturated zone water quality time lags at catchment scale. Agriculture, Ecosystems & Environment 236, 234–242. https://doi.org/10.1016/j.agee.2016.12.001

Vero, S.E., Ibrahim, T.G., Creamer, R.E., Grant, J., Healy, M.G., Henry, T., Kramers, G., Richards, K.G., Fenton, O., 2014. Consequences of varied soil hydraulic and meteorological complexity on unsaturated zone time lag estimates. Journal of Contaminant Hydrology 170, 53–67. https://doi.org/10.1016/j.jconhyd.2014.10.002

Viel, E., 2016. Etude des processus de transport des solutés hors équilibre physique: application à la zone non saturée des calcaires de Beauce. Thèse de doctorat. Université d'Orléans.

Wang, L., Stuart, M.E., Bloomfield, J.P., Butcher, A.S., Gooddy, D.C., McKenzie, A.A., Lewis, M.A., Williams, A.T., 2012. Prediction of the arrival of peak nitrate concentrations at

the water table at the regional scale in Great Britain. Hydrological Processes 26, 226–239. https://doi.org/10.1002/hyp.8164

Wellings, S.R., Bell, J.P., 1980. Movement of water and nitrate in the unsaturated zone of Upper Chalk near Winchester, Hants., England. Journal of Hydrology 48, 119–136. https://doi.org/10.1016/0022-1694(80)90070-0

Wesseling, J.G., Brandyk, T., 1985. Introduction of the occurrence of high groundwater levels and surface water storage in computer program SWATRE, Nota / Instituut voor Cultuurtechniek en Waterhuishouding;no. 1636. ICW, Wageningen.

Wesseling, J.G., Elbers, J.A., Kabat, P., Van den Broek, B.J., 1991. SWATRE: Instructions for input. Internal Note, Winand Staring Centre, Wageningen, the Netherlands.

Wood, T.R., Glass, R.J., McJunkin, T.R., Podgorney, R.K., Laviolette, R.A., Noah, K.S., Stoner, D.L., Starr, R.C., Baker, K., 2004. Unsaturated Flow through a Small Fracture–Matrix Network: Part 1. Experimental Observations. Vadose Zone Journal 3, 90–100. https://doi.org/10.2136/vzj2004.9000

Yates, S.R., Genuchten, M.T. van, Warrick, A.W., Leij, F.J., 1992. Analysis of Measured, Predicted, and Estimated Hydraulic Conductivity Using the RETC Computer Program. Soil Science Society of America Journal 56, 347–354. https://doi.org/10.2136/sssaj1992.03615995005600020003x

Zacharias, S., Bogena, H., Samaniego, L., Mauder, M., Fuß, R., Pütz, T., Frenzel, M., Schwank, M., Baessler, C., Butterbach-Bahl, K., Bens, O., Borg, E., Brauer, A., Dietrich, P., Hajnsek, I., Helle, G., Kiese, R., Kunstmann, H., Klotz, S., Munch, J.C., Papen, H., Priesack, E., Schmid, H.P., Steinbrecher, R., Rosenbaum, U., Teutsch, G., Vereecken, H., 2011. A Network of Terrestrial Environmental Observatories in Germany. Vadose Zone Journal 10, 955–973. https://doi.org/10.2136/vzj2010.0139

Zhang, Y., Schaap, M.G., 2019. Estimation of saturated hydraulic conductivity with pedotransfer functions: A review. Journal of Hydrology 575, 1011–1030. https://doi.org/10.1016/j.jhydrol.2019.05.058

Appendix A

Table A.1: Parameters θ_r, θ_s, α, n and K_s fitted with the MVG model using the RETC software for the vadose zone materials.

Sample	θ_r	θ_s	α	n	K_s	R^2	AICc
	[cm³/cm³]	[cm³/cm³]	[cm⁻¹]	[-]	[cm/d]	[-]	[-]
S_A	*0.000*	0.474 (0.421/0.526)	0.024 (0.017/0.031)	1.15 (1.12/1.18)	*30.24*	0.873	-140.5
S_B	*0.000*	0.466 (0.413/0.520)	0.024 (0.017/0.031)	1.16 (1.13/1.19)	*53.57*	0.866	-139.8
S_C	*0.000*	0.500 (0.433/0.567)	0.036 (0.014/0.059)	1.16 (1.12/1.20)	*47.52*	0.731	-143.0
P_A	*0.000*	0.451 (0.388/0.514)	0.025 (0.013/0.037)	1.17 (1.13/1.22)	*7.31*	0.924	-126.7
P_B	*0.000*	0.366 (0.329/0.403)	0.0073 (0.0043/0.0103)	1.25 (1.17/1.32)	*0.45*	0.921	-85.6
P_C	*0.000*	0.297 (0.277/0.317)	0.0031 (0.0010/0.0054)	1.22 (1.15/1.29)	0.14 (-0.05/0.33)	0.919	-107.7
P_D	*0.000*	0.353 (0.318/0.388)	0.0040 (0.0010/0.0073)	1.22 (1.13/1.31)	0.18 (-0.10/0.47)	0.894	-115.5
I_A	*0.000*	0.392 (0.343/0.440)	0.072 (0.052/0.091)	1.20 (1.14/1.26)	*35.22*	0.957	-96.3
I_B	*0.000*	0.370 (0.319/0.421)	0.160 (0.107/0.213)	1.23 (1.17/1.30)	*285*	0.939	-119.4
R_A	0.007 (-0.034/0.048)	0.298 (0.241/0.355)	0.516 (0.175/0.857)	1.36 (1.15/1.56)	*5000*	0.735	-120.7
R_B	*0.000*	0.155 (0.140/0.169)	0.015 (0.010/0.020)	1.16 (1.11/1.21)	*1.32*	0.962	-135.0
R_C	*0.000*	0.050 (0.048/0.053)	0.0014 (0.0008/0.0020)	1.23 (1.16/1.30)	0.0097 (0.0031/0.0163)	0.959	-177.2
R_D	*0.000*	0.095 (0.086/0.104)	0.0096 (0.0057/0.0134)	1.16 (1.10/1.23)	*0.40*	0.924	-147.2
R_E	*0.000*	0.117 (0.010/0.135)	0.127 (0.086/0.167)	1.15 (1.09/1.20)	*500*	0.949	-137.6
R_F	*0.000*	0.145 (0.125/0.166)	0.137 (0.097/0.177)	1.19 (1.13/1.24)	*500*	0.924	-132.6

Parameters highlighted in italics were fixed during the fitting procedure. Confidence intervals associated with parameters fitted using RETC are given in parentheses.

Table A.2: Parameters θ_r, θ_s, α, n and K_s fitted with the BBC model using the RETC software for the vadose zone materials.

Sample	θ_r	θ_s	α	n	K_s	R^2	AICc
	[cm³/cm³]		[cm⁻¹]	[-]	[cm/d]	[-]	[-]
S_A	*0.000*	0.531 (0.467/0.596)	0.212 (0.156/0.268)	0.118 (0.092/0.145)	*30.24*	0.896	-140.3
S_B	*0.000*	0.523 (0.453/0.594)	0.204 (0.148/0.60)	0.1256 (0.096/0.156)	*53.57*	0.885	-136.3
S_C	*0.000*	0.564 (0.456/0.669)	0.323 (0.080/0.566)	0.126 (0.087/0.165)	*47.52*	0.667	-130.1
P_A	*0.000*	0.447 (0.380/0.514)	0.048 (0.007/0.088)	0.149 (0.101/0.196)	0.24 (-0.04/0.53)	0.952	-121.5
P_B	*0.000*	0.367 (0.315/0.418)	0.017 (0.005/0.030)	0.199 (0.116/0.281)	0.090 (0.034/0.145)	0.939	-75.9
P_C	*0.000*	0.299 (0.273/0.325)	0.011 (0.005/0.017)	0.166 (0.109/0.224)	0.034 (0.010/0.069)	0.914	-100.2
P_D	*0.000*	0.362 (0.315/0.409)	0.015 (0.005/0.025)	0.161 (0.089/0.233)	0.054 (0.022/0.085)	0.858	-105.0
I_A	*0.000*	0.427 (0.355/0.500)	0.503 (0.324/0.682)	0.141 (0.089/0.194)	*35.22*	0.978	-88.8
I_B	*0.000*	0.423 (0.381/0.466)	0.999 (0.706/1.292)	0.185 (0.153/0.217)	*285*	0.954	-131.4
R_A	0.015 (-0.014/0.044)	0.319 (0.278/0.361)	0.959 (0.356/1.561)	0.362 (0.192/0.527)	*500*	0.870	-133.4
R_B	*0.000*	0.157 (0.137/0.177)	0.050 (0.002/0.098)	0.116 (0.060/0.171)	0.18 (-0.16/0.51)	0.966	-125.2
R_C	*0.000*	0.052 (0.047/0.059)	0.0081 (0.0044/0.0118)	0.133 (0.064/0.202)	*0.0055*	0.729	-154.1
R_D	*0.000*	0.096 (0.085/0.107)	0.027 (0.009/0.045)	0.127 (0.055/0.199)	0.034 (-0.007/0.075)	0.849	-138.7
R_E	*0.000*	0.108 (0.092/0.125)	0.064 (0.004/0.124)	0.158 (0.074/0.242)	1.28 (-1.03/3.60)	0.967	-131.7
R_F	*0.000*	0.136 (0.116/0.155)	0.083 (0.015/0.150)	0.200 (0.113/0.288)	2.48 (-1.50/6.46)	0.957	-128.1

Parameters highlighted in italics were fixed during the fitting procedure. Confidence intervals associated with parameters fitted using RETC are given in parentheses.

Table A.3: Simulated values of cumulative actual evapotranspiration (mm) and mean water storage (mm) and mean matric head (cm), water content (cm^3/cm^3) and water flux (cm/d) obtained at the observations nodes defined within the B2 profile with the MVG and DBM models.

Depth (m)	Material (Borehole)		B1	B2	B3
		Cumulative ET_R	28110	28009	28296
		Water Storage	4082	3932	3987
0.3	S_A (B1-B2-B3)	h	-1578.6	-1620.6	-1485.9
		θ	0.3398	0.3390	0.3412
		Water Flux	-0.0422	-0.0428	-0.0414
0.6	S_B (B1-B2-B3)	h	-834.6	-890.1	-715.5
		θ	0.3557	0.3551	0.3585
		Water Flux	-0.0344	-0.0350	-0.0336
0.9	S_C (B1-B2-B3)	h	-611.6	-669.2	-444.8
		θ	0.3939	0.3920	0.3988
		Water Flux	-0.0343	-0.0348	-0.0334
1.2	P_A (B1-B2) S_C (B3)	h	-207.2	-153.3	-321.7
		θ	0.3611	0.3643	0.4027
		Water Flux	-0.0344	-0.0350	-0.0335
2.5	P_B (B1-B2-B3)	h	-68.1	-67.9	-89.4
		θ	0.3316	0.3321	0.3289
		Water Flux	-0.0343	-0.0350	-0.0334
3.3	P_C (B1-B3) P_B (B2)	h	-61.2	-58.5	-76.0
		θ	0.2856	0.3331	0.2846
		Water Flux	-0.0344	-0.0350	-0.0336
6.0	I_B (B1) P_D (B2-B3)	h	-45.2	-45.9	-49.9
		θ	0.2060	0.3266	0.3261
		Water Flux	-0.0344	-0.0348	-0.0335
8.0	R_B (B1-B2-B3)	h	-49.9	-57.5	-51.6
		θ	0.1388	0.1379	0.1386
		Water Flux	-0.0343	-0.0348	-0.0335
10.0	R_D (B1-B2-B3)	h	-20.1	-21.1	-23.1
		θ	0.0903	0.0900	0.0895
		Water Flux	-0.0342	-0.0347	-0.0334
14.6	R_E (B1-B2-B3)	h	-73.0	-71.9	-75.8
		θ	0.0818	0.0819	0.0816
		Water Flux	-0.0341	-0.0346	-0.0333

Table A.4:		h	19.2	11.3	Simulated
	11.2	θ	0.094	0.103	
values of		Water Flux	-0.0243	-0.0346	cumulative
		h	-33.4	-21.7	
actual	11.4	θ	0.050	0.049	
		Water Flux	-0.0243	-0.0347	
		h	-106.8	-71.9	
	14.6	θ	0.080	0.082	
		Water Flux	-0.0242	-0.0346	

evapotranspiration (mm) and mean water storage (mm) and mean matric head (cm), water

content (cm^3/cm^3) and water flux (cm/d) obtained at the observations nodes defined within the

B1, B2 and B3 profiles with the DBM model.
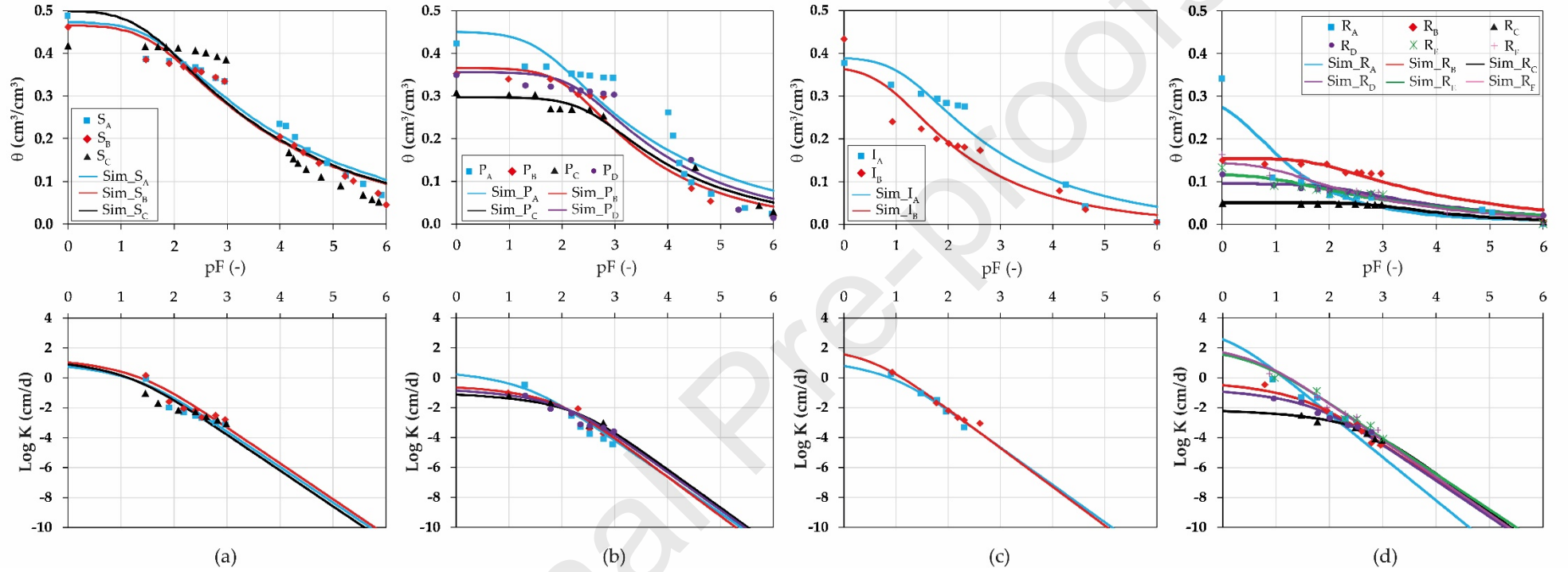
Appendix B:

Figure B.1: Comparison between experimental and fitted (MVG model) water retention ($\theta(h)$, up) and hydraulic conductivity ($K(h)$, down) curves

for the soil (a), powdery limestone (b), calcareous sand (c) and limestone rock (d) samples.
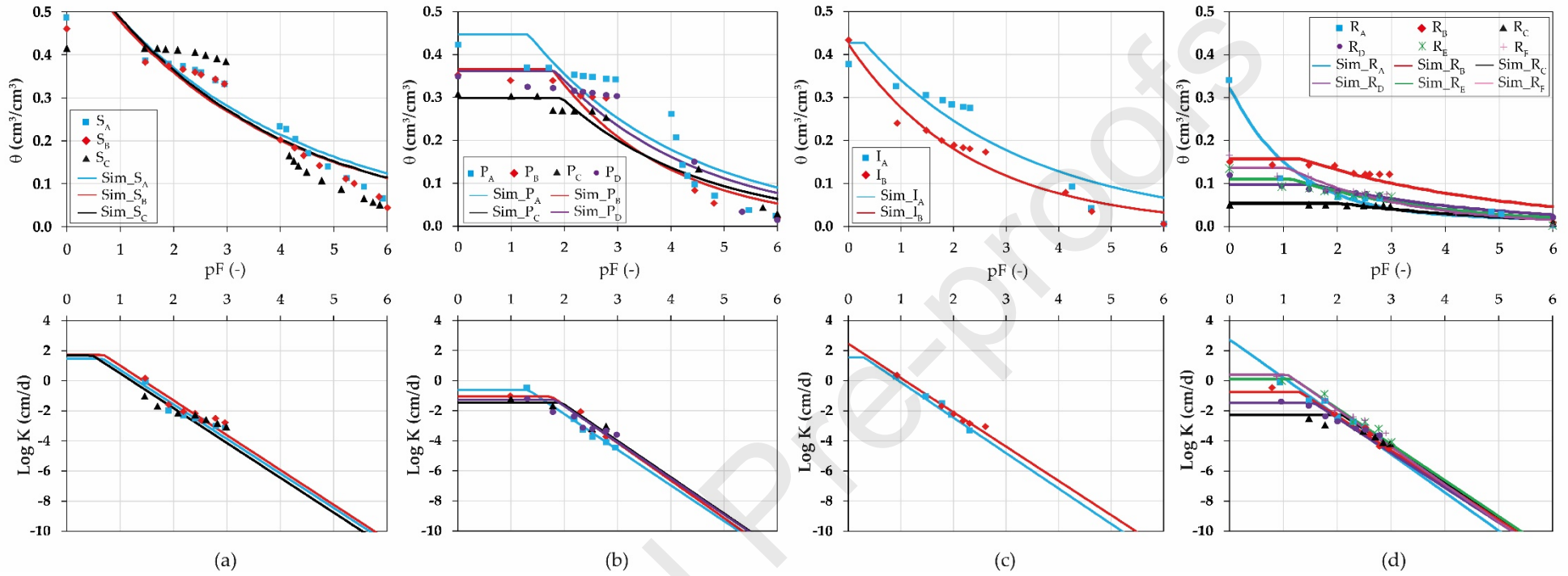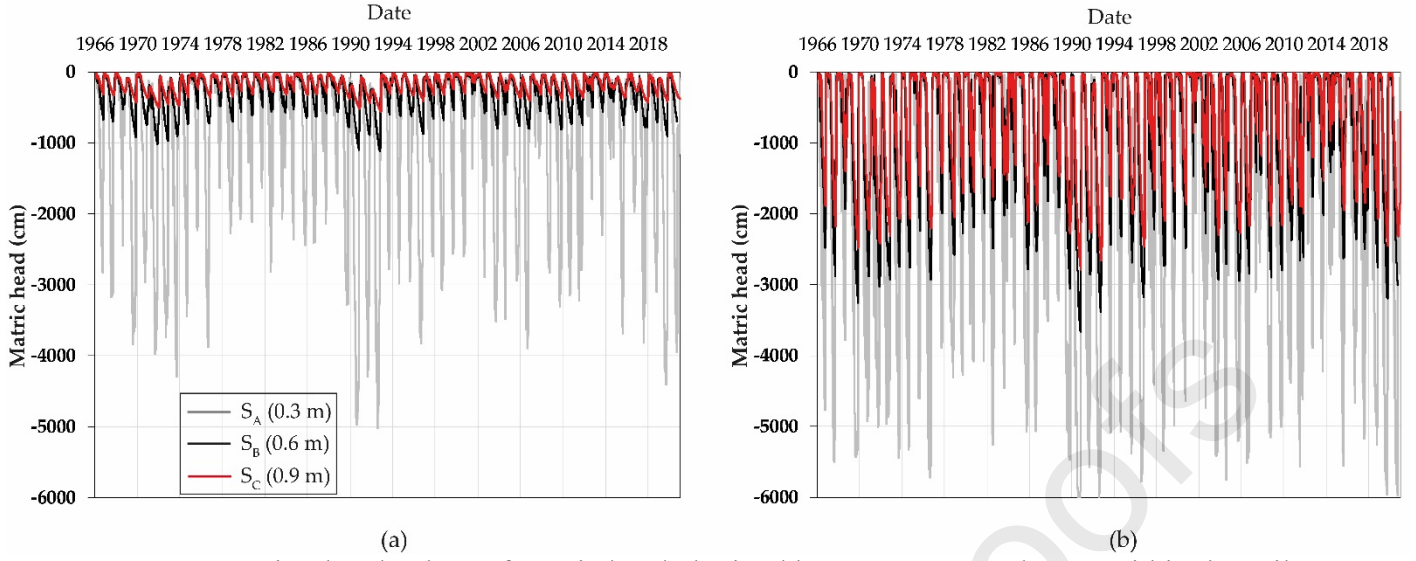
Figure B.2: Comparison between experimental and fitted (BBC model) water retention ($\theta(h)$, up) and hydraulic conductivity ($K(h)$, down) curves for the soil (a), powdery limestone (b), calcareous sand (c) and limestone rock (d) samples.

Figure B.3: Simulated values of matric head obtained between 1966 and 2020 within the soil

layers of the B2 profile with the MVG (a) and DBM (b) models.
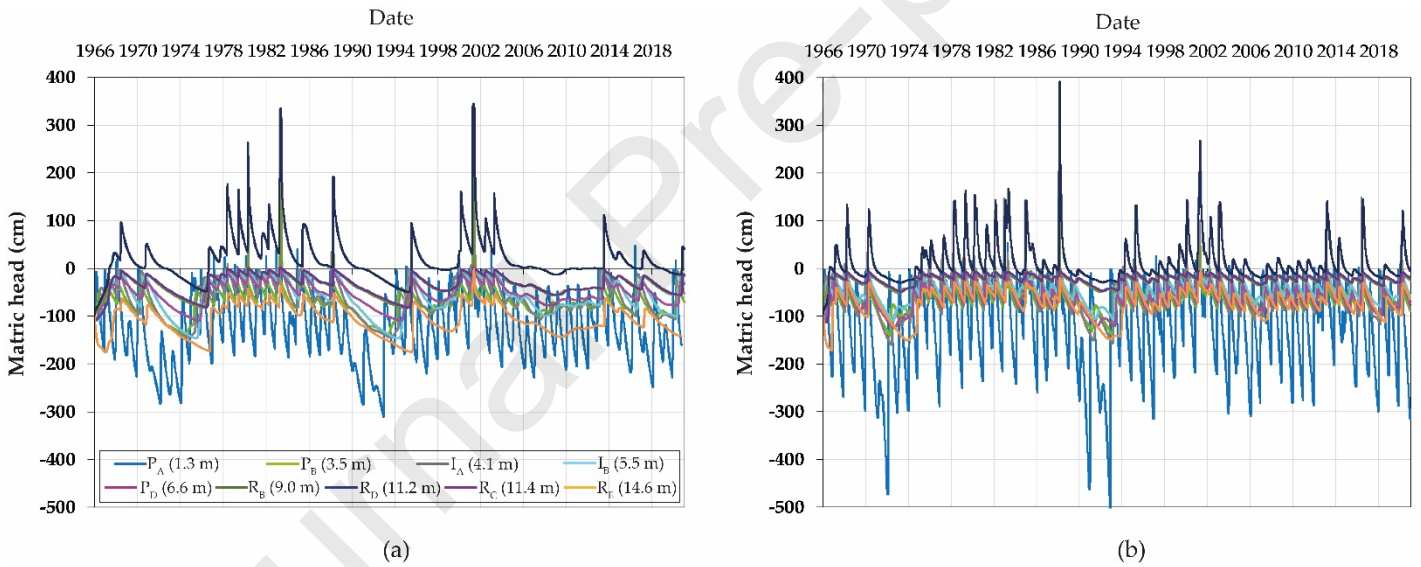

Figure B.4: Simulated values of matric head obtained between 1966 and 2020 at the

observation nodes defined for the B2 profile with the MVG (a) and DBM (b) models.
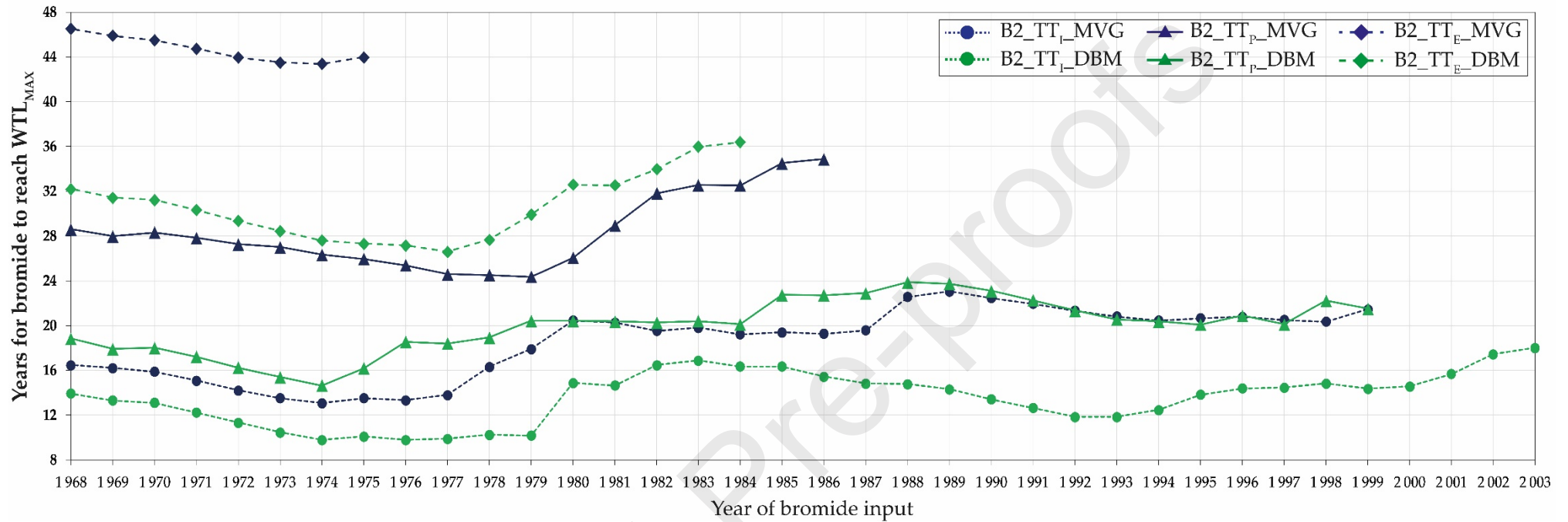
Figure B.5: TT_I (dotted line, down), TT_P (solid line) and TT_E (dotted line, up) estimated from the simulation of bromide transport within the B2

profile down to WTL_{MAX} (-14.60 m) with the MVG and DBM models as a function of the year of the input.
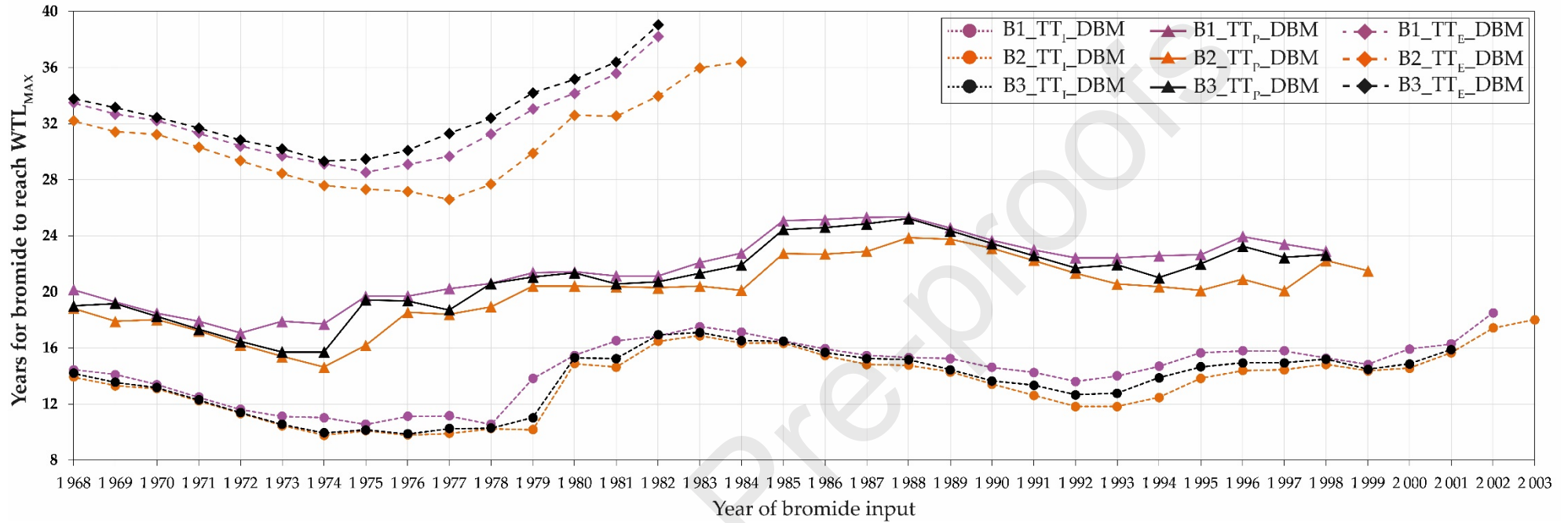
Figure B.6: TT_I (dotted line, down), TT_P (solid line) and TT_E (dotted line, up) estimated from the simulation of bromide transport within the B1,

B2 and B3 profiles down to WTL_{MAX} (-14.60 m) with the DBM model as a function of the year of the input.

Figure 1: Localization of the experimental site, distance between the three cored boreholes (B1, B2 and B3) and position of the soil pit.

Figure 2: Annual mean temperature, rainfall and ETP, and daily water table level observed from 1966 to 2020.

Figure 3: Comparison between experimental and fitted (DBM model) water retention ($\theta(h)$, up) and hydraulic conductivity ($K(h)$, down) curves

for the soil (a), powdery limestone (b), calcareous sand (c) and limestone rock (d) samples.

Figure 4: Comparison between measured water content profiles for B1 (a), B2 (b) and B3 (c) at the date of the drilling (14 March 2017) and those simulated by the models (DBM for B1 and B3 and MVG and DBM for B2).

Figure 5: Simulated values of matric head obtained between 1991 and 1994 (dry VZ profile with WTL_{MIN} = -22.21 m on 19/08/1992, up) and between 2000 and 2003 (wet VZ profile with WTL_{MAX} = -14.60 m on 15/05/2001, down) at the observation nodes defined for the B2 profile (Table 1) with the MVG (a) and DBM (b) models.

Figure 6: Bromide concentration simulated at 0.9 (a), 3.5 (b), 6.6 (c) and 14.6 m (WTL_{MAX}) (d) deep by the MVG and DBM models in the B2 profile and as a function of the years after input. Two input years are presented, corresponding to small (1977, up) and large (1989, down) travel time.

Figure 7: Simulated values of matric head obtained between 1991 and 1994 (dry VZ profile with WTL_{MIN} = -22.21 m on 19/08/1992, up) and between 2000 and 2003 (wet VZ profile with WTL_{MAX} = -14.60 m on 15/05/2001, down) at 0.9 (a), 3.3 (b), 10.0 (c) and 14.6 (d) m deep within the B1, B2 and B3 profiles with the DBM model.

Figure 8: Bromide concentration simulated at 1.2 (a), 3.5 (b), 8.0 (c) and 14.6 m (WTL_{MAX}) (d) deep by the DBM model in the three VZ profiles (B1, B2 and B3) as a function of the years after input. Two input years are presented, corresponding to small (1977, up) and large travel time (1989, down).

Figure 9: Optical imaging of five new boreholes (B5, B6, B7, B8 and B9 drilled in Spring 2020 at a few tens meters from B1, B2 and B3) highlighting fractures and karstification processes observed between 12.6 and 13.5 m deep in the rock formation of the Beauce limestone aquifer.

Figure B.1: Comparison between experimental and fitted (MVG model) water retention ($\theta(h)$, up) and hydraulic conductivity ($K(h)$, down) curves for the soil (a), powdery limestone (b), calcareous sand (c) and limestone rock (d) samples.

Figure B.2: Comparison between experimental and fitted (BBC model) water retention ($\theta(h)$, up) and hydraulic conductivity ($K(h)$, down) curves for the soil (a), powdery limestone (b), calcareous sand (c) and limestone rock (d) samples.

Figure B.3: Simulated values of matric head obtained between 1966 and 2020 within the soil layers of the B2 profile with the MVG (a) and DBM (b) models.

Figure B.4: Simulated values of matric head obtained between 1966 and 2020 at the observation nodes defined for the B2 profile with the MVG (a) and DBM (b) models.

Figure B.5: TT_I (dotted line, down), TT_P (solid line) and TT_E (dotted line, up) estimated from the simulation of bromide transport within the B2 profile down to WTL_{MAX} (-14.60 m) with the MVG and DBM models as a function of the year of the input.

Figure B.6: TT_I (dotted line, down), TT_P (solid line) and TT_E (dotted line, up) estimated from the simulation of bromide transport within the B1, B2 and B3 profiles down to WTL_{MAX} (-14.60 m) with the DBM model as a function of the year of the input.

- ✓ Simulation of water flow and TT in the VZ using unimodal and bimodal approaches

- ✓ Parameterization of HYDRUS-1D using hydraulic properties laboratory measurements

- ✓ Experimental hydraulic properties were more accurately described with the DBM model

- ✓ Results obtained with unimodal and bimodal models presented strong differences

- ✓ Large influence of VZ vertical heterogeneity and meteorological conditions